Combining multi-physical measurements to quantify bedload transport and morphodynamics interactions in an Alpine braiding river reach

Clément Misset, Alain Recking, Cédric Legout, Maarten Bakker, Nathan Bodereau, Laurent Borgniet, Mathieu Cassel, Thomas Geay, Florent Gimbert, Oldrich Navratil, et al.

COMBINING MULTI-PHYSICAL MEASUREMENTS TO QUANTIFY BEDLOAD TRANSPORT AND MORPHODYNAMICS INTERACTIONS IN AN ALPINE BRAIDING RIVER REACH

Authors

C. Misset[1]*, A. Recking[1], C. Legout[2], M. Bakker[1,2], N. Bodereau[1], L. Borgniet[1], M. Cassel[3], T. Geay[4], F. Gimbert[2], O. Navratil[5], H. Piegay[3], N. Valsangkar[1], M. Cazilhac[6], A. Poirel[6] and S. Zanker[6]

[1] Univ. Grenoble Alpes, Irstea, ETNA, Grenoble, France

[2] Univ. Grenoble Alpes, CNRS, IRD, Grenoble INP, IGE, Grenoble, France

[3] Univ. Lyon, UMR CNRS 5600 EVS, Lyon, France

[4] Univ. Grenoble Alpes, CNRS, Grenoble INP, GIPSA-lab, Grenoble, France

[5] Univ. Lumière Lyon 2, UMR 5600-CNRS Environnement Ville Société, Bron, France

[6] EDF, DTG, Grenoble, France

* Corresponding author

ABSTRACT

Understanding the interactions between bedload transport and morpholdynamics in braided streams has important applications in river management and restoration. Direct field measurements addressing this question are however scarce as they are often challenging to perform. Here, we report an extensive two-month field campaign in an Alpine braided reach (La Séveraisse river, French Alps) that experienced predictable daily peak discharge (48 events observed) generating significant bedload transport and morphological changes during the melting season. We monitored these processes using a wide range of direct and indirect techniques (bedload sampling, continuous seismic measurements, pebbles tracking, topographic surveys, remote sensing using ground control cameras and drone flights). Doing so, surrogate measurements allowed to extend temporally discrete manual bedload sampling, and to extend spatially local riverbed cross section measurements. These measurements provide unique complementary constraints on the targeted physics, at various spatial and temporal scales which enabled us to draw robust conclusions. Data showed a progressive decrease in bedload transport for a given flow rate along the two months period. Simultaneously, river morphology in the braided sections changed from an incised to a more distributed configuration which led to a decrease of local maxima in dimensionless shear stresses in the braided reach for similar flow conditions. This control of bedload transport by maximum local shear stresses was in line with tracked pebble surveys indicating that coarse bedload particles were mostly transported in the main active channel. At the reach scale, this transport was found to be more efficient in laterally confined sections than in braided ones which has important implications in terms of bedload estimation in alternative confined and braided (unconfined) rivers. Finally, this study highlight the interest to combine a large variety of traditional and innovative measurements techniques to better understand complex sediment transport processes in the field.

1. INTRODUCTION

In Alpine environments, sediment supplied from hillslopes is generally transferred through the river system via a complex cascade of processes. Sediment passes through successive types of riverbed morphologies [*Montgomery and Buffington*, 1997], each of which affecting transfer efficiency due to changes in river bed characteristics [*Recking et al.*, 2016]. Among these, braiding river reaches play a key role due to their high capacity to store sediments in terraces, bars, and channels [*Hoey*, 1992; *Lisle and Church*, 2002; *Wilkinson et al.*, 2006]. Braided rivers are present in various settings [*Surian*, 2015]. They are characterized by multiple channels, separated by unstable bars, that interact with one another at confluences and bifurcations of the flow [*Ashmore*, 1991]. In mountainous areas, river systems often show alternating braiding and non-braiding reaches (Figure 1) and it is unclear how each of these morphologies impact the transfer of bed material. As a consequence, understanding the relation between bedload transport rates and braiding morphology is a keystone for river management and restoration programs. The study of braided reaches is not only useful for the braided reaches themselves, but also further downstream, where river morphological development depends strongly on the upstream storage and release of sediment.

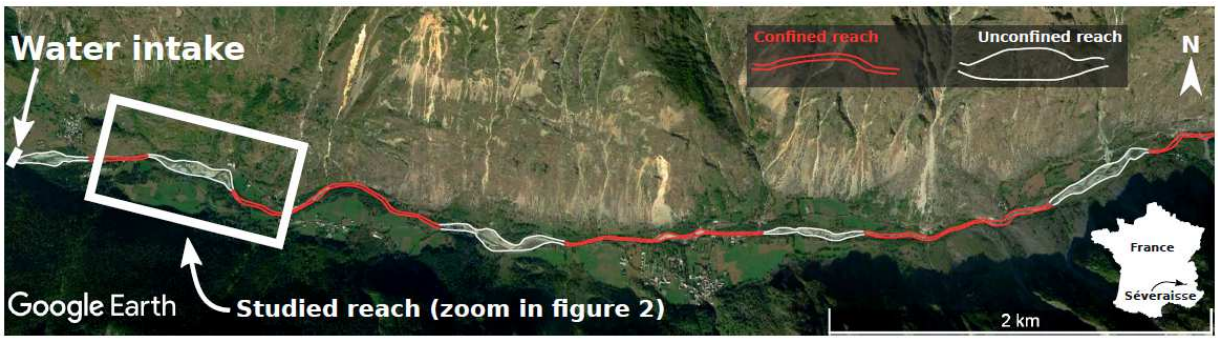

Figure 1: Braided reaches (white lines) alternating with narrow confined reaches (black lines) in the Séveraisse river (Google earth 2016). A water intake is located downstream the study area.

Conditions for braiding are related to a high supply of bedload material, low bank resistance and limited in-channel riparian vegetation [*Bertoldi et al.*, 2011; *Eaton et al.*, 2010; *Gran and Paola*, 2001]. Braided morphology observed at a given time results from

complex interactions between the river morphology, the hydraulic conditions, and the solid flux. Thus, large fluctuations in bedload fluxes have been observed in flume experiments for constant water discharge [*Ashmore*, 1988; *Gomez et al.*, 1989; *Recking et al.*, 2009]. Average cross section hydraulic parameters (stream power or bed shear stress) are typically used for bedload transport modeling in single channel morphologies when there are no available measurements. However, this approach leads to large under-predictions of bedload fluxes in flume experiment of braiding morphologies [*Bertoldi et al.*, 2009a]. This is likely due to bedload transport being localized in narrow zones within the cross section where shear stresses are high [*Warburton*, 1992; *Williams et al.*, 2015], which is not well captured by the averaged hydraulic parameters [*Bertoldi et al.*, 2009a; *Ferguson*, 2003; *Nicholas*, 2000; *Paola*, 1996; *Recking*, 2013a]. Also, for successive braiding-confined morphologies in the field, the choice of the cross section where bedload equations should be applied is poorly documented and may lead to large uncertainties in such streams [*Recking et al.*, 2016]. In addition, it has been observed that depending on the upstream bedload fluxes, braided rivers may experience aggradational or degradational phases [*Liebault et al.*, 2013]. During aggradation, a decrease in flow depth for a given flow rate reduces the capacity of the channel to export bed material while during degradation, the flow concentrates in incised channels, leading to increased transport capacity [*Pryor et al.*, 2011]. These observations support the notion that there is no single relationship between the water discharge and transport capacity in such streams and that morphological changes have strong and direct effects on bedload transport.

Although the relation between bedload transport and braiding morphodynamics has been investigated for decades using flume experiments [*Ashmore*, 1982; *Bertoldi et al.*, 2009a; *Warburton and Davies*, 1994] few field studies such as the one of Lane *et al.* (1996) reported simultaneous bedload transport and braiding morphodynamics measurements. This lack of field observations of bedload transport is largely due to difficulties associated with direct sampling being highly challenging in such highly dynamic streams with unstable bed morphology. It is particularly true for large braided systems as reported in previous well known studies on the Tagliamento river in Italy [*Bertoldi et al.*, 2009b; *Mao and Surian*, 2010], the Rees river in New Zealand [*Williams*

et al., 2014; *Williams et al.*, 2016] or the Sunwapta river in Canada [*Ashmore et al.*, 2011; *Middleton et al.*, 2019] where direct sampling are not feasible. This limitation led to the use of remote sensing technics such as photogrammetry [*Bakker and Lane*, 2017; *Lane et al.*, 1996; *Lane et al.*, 2003], lidar [*Bertoldi et al.*, 2011; *Lallias-Tacon et al.*, 2014; *Milan et al.*, 2007] or ground-based imagery [*Ashmore et al.*, 2011; *Luchi et al.*, 2007] to specifically study morphological changes in these braided streams and deduce minimum bedload fluxes using the morphological method [*Ashmore and Church*, 1998]. On the other hand, few studies have focused on the measurement of bedload transport in braiding rivers by using classical sampling methods when feasible [*Meunier et al.*, 2006], indirect seismic measurements [*Burtin et al.*, 2011], ADCP survey in wetted channels [*Williams et al.*, 2015] or pebble tracers to detect bedload particle path and bedload flux using the virtual velocity method [*Chapuis et al.*, 2015; *Liébault et al.*, 2012; *Mao et al.*, 2017]. Direct samplings give an estimate of transport and topography respectively, but with limited time and space resolution. Surrogate techniques give access to large temporal and spatial observations, but need calibration with local measurements [*Gray et al.*, 2010].Thus combining direct and indirect techniques permits to optimize field-based measurements.

In this paper, we present a comprehensive measurement campaign in an Alpine braided river reach (La Séveraisse, Ecrin Massif, SE French Alps). Daily floods of various magnitudes occur each year during a 2-month snowmelt season (May to June). Such regular seasonal and daily occurrence allow preparing the field campaigns and to test a combination of techniques/approaches that can most of the time not be combined in the same field during the same period. Then traditional and novel techniques were used to conduct complementary hydrological and sediment transport measurements (bedload sampling, continuous seismic measurements, pebbles tracking, topographic surveys, remote sensing using ground control cameras and drone flights). Those measurements have been made at several key places throughout the reach and continuously. The objectives of the study were: i) to assess the interest of such multi-physical measurement approach and its application in future geomorphological studies; ii) to provide new insights into characterizing bedload transport and braided bed morphology

dynamics during the course of a snow-melt season; and (iii) to analyze relations between the various physical quantities, confronting them with predictive formulas.

2. STUDY AREA

The Séveraisse catchment in the Ecrin Massif (SE French Alps) is well suited for this study because it has low-human impact (no dams or water intakes upstream the study area, limited embankments), it is well-accessible from the river banks, and it provides opportunities for direct bedload sampling from bridges (Figure 2). At the gauging station (managed by EDF, a French electric power company), the drainage area is 130 km². The valley morphology is shaped by glacial erosion and the river is still fed by glaciers located in the upper parts of the catchment (maximum elevation of 3579 m a.s.l). The geology mainly comprises crystalline rocks (gneiss, granite) and few patches of softer rocks (marls). The upper part of the catchment is highly erosive and delivers large amounts of sediment via rock falls, debris flows [*Helsen et al.*, 2002] and tributaries. These areas are well-connected with downstream river reaches, showing several sequences of well-developed braiding morphologies and straight (confined) river channels in the more laterally-confined sections of the valley. In this study we considered a confined-braided-confined sequence located few hundred meters upstream of the gauging station (Figure 2).

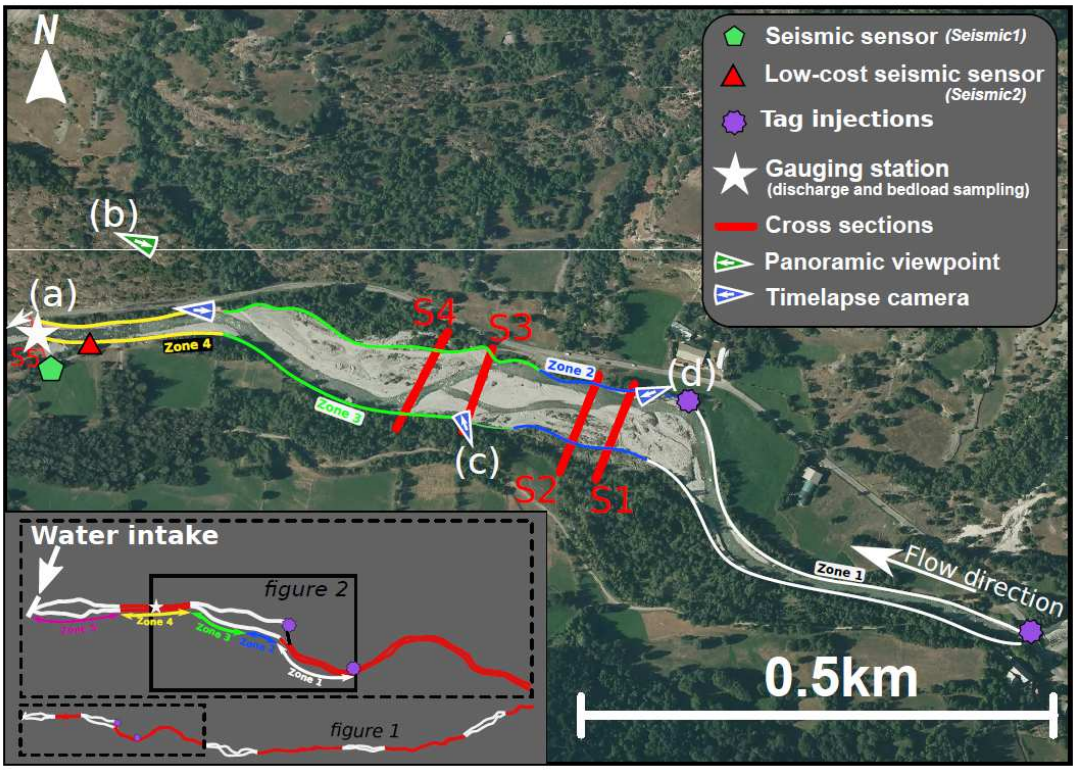
N
Seismic sensor (Seismic1)
Low-cost seismic sensor (Seismic2)
Tag injections
Gauging station (discharge and bedload sampling)
Cross sections
Panoramic viewpoint
Timelapse camera
(a)
(b)
(c)
(d)
S1
S2
S3
S4
S5
Zone 1
Zone 2
Zone 3
Zone 4
Water intake
figure 1
figure 2
Flow direction
0.5km

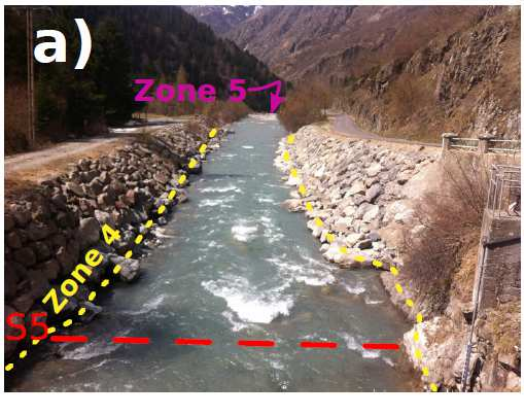
a)
Zone 5
Zone 4
S5

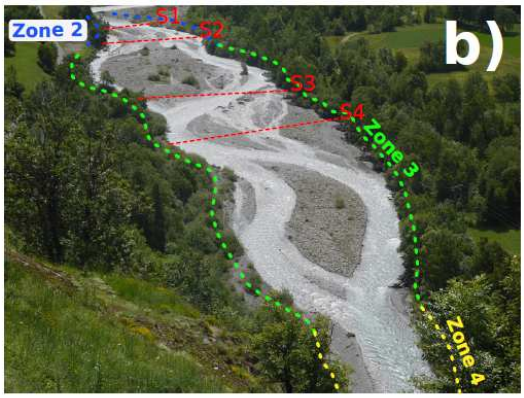
b)
Zone 2
S1
S2
S3
S4
Zone 3
Zone 4

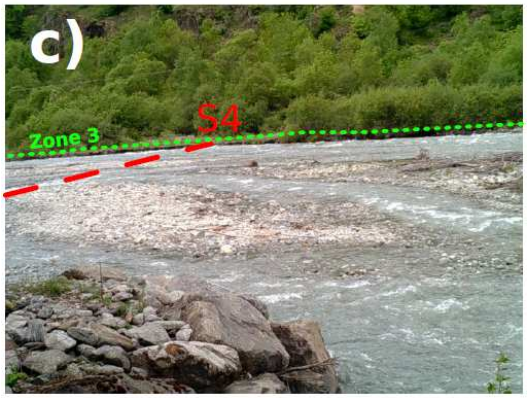
c)
Zone 3
S4


d)
S1
Zone 2
S2

Figure 2 : Location of the instruments and measurements within the studied reach of the Séveraisse. S1 to S5 correspond to cross-section surveys located from upstream to downstream; (a) is the narrow and paved downstream section were flow rate measurements and bedload sampling were performed (station location: Lat 44.824502°, Long 6.149043°), (b) is a view of the braided reach, (c) is a picture taken from a time-lapse camera in the middle of the braided reach and (d) is a picture taken from a time-lapse camera in the upstream part of the braided reach. The five zones used to analyze tracking pebble surveys are indicated with different colors. These zones have different morphologies: zone 1 and 4 are narrow and confined, zone 2 is the entrance of the braided reach, and zone 3 is the downstream part of the braided reach. Zone 5 is located downstream the gauging station few meters upstream the water intake and is the most downstream prospected zone.

3. MATERIAL AND METHODS

3.1. DIRECT BEDLOAD TRANSPORT SAMPLING

Bedload fluxes were sampled downstream from the studied reach (S5 in Figure 2), on the bridge besides the gauging station which provided discharge measurements (repeated gauging using dilution, ADCP, velocity profilers techniques and coupled with continuous pressure level sensors at 10 min time-interval). No change in the rating curve was observed as confirmed by daily bed topography controls performed by the field team. A pressure difference sampler (Elwha 20.7×12 centimeter) with a mesh size of 0.5 mm was deployed at approximately 1.5 m intervals across the channel width. The bedload flux was integrated over the cross section using Eq.1:

$$q_b = \frac{1}{L_t} \sum_{i=1}^{N} \frac{Q_{be\,i}}{L_e} L_i \qquad (1)$$

in which q_b is the bedload rate per unit width (g s^{-1} m^{-1}), N is the number of samples, $Q_{be\,i}$ is the bedload rate for each sample (g s^{-1}), L_t is the cross section width (m), L_e is the sampler width (m) and L_i is the width considered representative for the sampling point i (m). The time of sampling (from 15 to 300 seconds) was adapted to bedload transport conditions to avoid trapping efficiency deceases. Between the 27th of April and the 26th of June, 60 measurements of the cross-sectional bedload flux (q_b) were performed. These measurements were performed for a wide range of water discharges

(9-25 m^3/s), allowing us to elaborate rating curves and to observe temporal changes in bedload rates. A resampling technique detailed in Appendix C was used to test the significance of temporal trend in bedload samples. This method is based on an analysis of the relation between time and residuals obtained from a power law fitted between bedload and the flow rate.

The cross-sectional bedload grain-size distribution was measured for a subset of the samples (17 of the 60 samples). We mainly focused on samples collected in the central part of the cross section with the largest unit bedload rates. Bed load samples were sieved with 1.6mm, 10mm, 20mm, 32mm, 45mm, 64mm, 91mm, 128mm and 181mm mesh sizes. The 50^{th} and 84^{th} percentiles of the transported diameters in terms of mass could then be calculated (D_{50} and D_{84}).

3.2. INDIRECT BEDLOAD TRANSPORT MEASUREMENTS

To complement the previous direct in-stream sampling, we performed continuous, indirect measurements based on seismic monitoring to assess the variability of bedload transport in time [*Burtin et al.*, 2008; *Burtin et al.*, 2011; *Cook et al.*, 2018]. In this study, we used two types of seismic measurements with geophones: (i) a setup classically used in this context (e.g. Cook *et al.* (2018)) in which the full high frequency (<400 Hz) waveform is saved continuously (called Seismic1 at Figure 2) and (ii) a seismic device initially developed for debris-flows monitoring applications, in which a temporally and frequency averaged proxy for ground motion velocity is saved instead of the full ground velocity waveform (Seismic2) [*Bel et al.*, 2017; *Navratil et al.*, 2013]. The geophones allow ground-motion vibrations to be investigated within the range ca. 5-200 Hz which encompasses frequencies expected for bedload transport [*Gimbert et al.*, 2019; *Tsai et al.*, 2012] and flow turbulence [*Gimbert et al.*, 2014].

At Seismic1, the classical seismic station, a PE-6/B geophone was installed on the river floodplain (25 m from the left channel bank, Figure 2) to monitor bedload-induced seismic vibrations. The data was recorded with a frequency of 400 Hz on a DiGOS DATA-CUBE^3. Given that bedload-induced noise is thought to be of a higher frequency

than turbulent-flow-induced noise [*Cook et al.*, 2018; *Gimbert et al.*, 2014] we calculated seismic power P_b at relatively high frequencies. We evaluate P_b in the 20-80 Hz frequency range allowing maximum sensitivity to bedload while minimizing the contribution of strong site effects (anthropogenic noise) at the very high frequencies (> 100 Hz). If primarily caused by bedload, seismic power P_b is set by impact forces exerted by transported bed material on the river bed, and is expected to scale with bedload flux (Q_b) and transported grain diameter (D) as [*Tsai et al.*, 2012]:

$$P_b \sim Q_b \times D^3 \quad (2)$$

At Seismic2, a seismic monitoring station developed for debris flow monitoring was installed close to the main channel, on the left river bank (few meters from the main channel, 40m upstream the gauging station, Figure 2) with a solar panel power-supply and a vertical geophone GS20-DX Geospace® (8 Hz natural frequency). This low-cost and low-power consumption station has the advantage to allow seismic recording during long time-period in remote environmental conditions with limited field maintenance. A three-step signal conditioning was performed with an electronic interface [*Navratil et al.*, 2013]: i) the signal of the geophone is rectified; ii) a low-pass filter (from f_c=0.5Hz to 80Hz) is applied; iii) the signal is amplified and finally recorded (5-Hz sampling frequency) with a Arduino Uno® open-source microcontroller. The signal amplitude (in mV) thus directly derived from the seismic energy integrated in the frequency band 0-80Hz.

3.4. COARSE PARTICLES DISPLACEMENT

To quantify the transport and mobility of coarse particles in the braiding stream, 29 natural pebbles were equipped with active ultra-high frequency transponders, also known as a-UHF tags [*Cassel et al.*, 2017a]. Their average *b*-axis is 77mm, approximately twice the D_{50} value of the study site. The transponders were of the COIN-ID model, emitting a beacon signal at 433.92 MHz every 2.2s. The tags were placed into a 40mm diameter hole drilled in the pebbles and then filled with the mixture polyurethane resin and corundum [*Cassel et al.*, 2017b]. Sediment tracers were injected

on the 12th of June 2018 at two locations on the study site. Fifteen tracers were injected in a narrow section located 500 meters upstream the entrance of the braided reach. Fourteen of them were injected from the embankment in the river bed a few meters upstream the entrance of the studied reach (Figure 2). Following tracer injection, 5 tracking-surveys were conducted within a period of 2 weeks (Table 1). The first three periods covered one water discharge peak and the following two a series of 4 and 6 peaks respectively.

	Injection	**Tracking**				
Date	12/06/18 (Am)	12/06/18 (Pm)	13/06/18 (Day)	14/06/18 (Day)	18/06/18 (Day)	25/06/18 (Day)
Prospected zones	-	Partial (Z1 and Z2)	Full	Full	Partial (Z1 to Z4)	Full
Recovery rate	29/29 (100%)	13/29 (45%)	21/29 (72%)	22/29 (76%)	23/29 (79%)	25/29 (86%)
Number of peaks discharge	-	1	1	1	4	6
Maximum peak dischage (m^3/s)	-	19.5	22.6	20	19.5	24.2

Table 1: Synthesis of the pebbles tracking campaign. There were five prospection zones, Z1 to Z5 from upstream to downstream. Zones Z1 to Z4 are indicated in Figure 2.

The tracers were tracked using a reading system (composed of a Slender III antenna and SCIEL reader connected at laptop) and a GPS (Leica Zeno 20), carried by three operators, from the main channel banks (Figure 2a). The antenna (370mm×370mm×40mm, aperture angle of 80° characterized by an isotropic gain and a mass of approximately 1.5kg) was moved and oriented such as to maximize the a-UHF tag signal intensity by real-time visual monitoring of the received signal strength indication (so called RSSI). The main advantages of this method are its rapidity, allowing prospection of the entire study reach between two floods event, and its detection range, estimated at 10m for transponders immerged in 50cm of water and about 40m in the open field [*Cassel et al*., 2017a]. The tracer localization was performed in a single longitudinal profile along the river as proposed by Piégay *et al.* (2016), with an

uncertainty of approximately 10m. Therefore, an uncertainty of 20m was considered for the tracers 1D travelled distance between surveys. In the braided sections, the antenna was moved from both banks so that the entire channel width was surveyed which allowed us to determine if tracers were located in secondary channels or in the main one. The data of the travelled distance are analyzed with respect to the tracer injection locations, the zones of the study reach where tracers have been deposited or entrained and the duration between tracking surveys to determine virtual velocities, as well as the channel in which they traveled.

3.5. QUANTIFYING MORPHOLOGICAL CHANGES

Repeated topographical surveys were conducted along five cross-sections (S1 to S5; Figure 2) to quantify the morphological changes over the snow melting period. A topographic total station (Leica Geosystems) was used with fixed marks on both banks allowing accurate morphological comparison through time. Measurements were performed during low-flow periods for safety reasons. Vertical resolution of the measurements is limited to the size of the coarse bed-particles. It is estimated to be approximately ca.10 cm (twice the median surface particle size D_{50}). Non-truncated Wolman pebble counts of surface grain-size were also performed at the beginning and at the end of the campaign to detect potential grain-size changes associated with morphological changes. Each time, four hundred particles were sampled along four transects (two in the main channel and two on top of bars) approximately located at the same positions.

Three cameras, similar to the ones used by Benacchio *et al.* (2017) were installed to record local morphological changes at the upstream, middle, and downstream locations of the braided reach (Figure 2). Pictures were taken every 20 min from 6 AM to 10 PM. In addition, several pictures were taken (n=4) from a vantage point at the downstream end of the reach to qualitatively observe morphological changes (Figure 2a).

To characterize global morphological changes, two drone flights were performed before and after the melting season on respectively the 27th of April and 25th of July. We

assume that morphological changes that occurred after the field campaign were limited in comparison to those occurring during this period as only one significant ($Q=17m^3/s$) and three other lower intensity ($Q<15m^3/s$) peak discharges were recorded in July. A drone-based camera (ILCE-7, focal length 35 mm, resolution 6000×4000) was used to take pictures (respectively 426 and 676 in April and July) with an overlap of minimum 85%, enabling the reconstruction of orthorectified images with a 2cm-resolution. Images were aligned by using Structure from Motion photogrammetry software (Agisoft Photoscan) and c. 30 ground control points measured in the field using a differential GPS. GPS point's accuracy (3D position) was on average 1.6 cm. The accuracy on 2D position (XY) of the orthorectified images obtained (estimated by the root mean squared errors of ground control points used in orthorectification) was respectively 10.3 and 10.1 cm in April and July. A laserScan (Yellowscan) installed under the drone was also used to performe a scan of the river bed to construct digital elevation models (DEMs) and calculate the elevation differences between the two fights. An average point density of 60 points/m^2 was obtained. DEMs were filtered, aligned and their elevation difference was calculated on a 1m-radius using Cloud Compare software considering a 25cm-limit of detection. This technique based on laser scanning provides elevations for exposed surfaces. Consequently, it cannot detect topographic changes occurring within the wetted channels.

3.6. HYDRAULIC CALCULATIONS

To estimate the main hydraulic parameters (velocity, hydraulic radius and water depth) at the five surveyed cross sections (S1 to S5) from the measured discharge Q, we used the flow resistance equation proposed by Ferguson (2007) (detail in Appendix A) by iteratively adjusting water level, assumed to be uniform over the cross section, and using a mean reach slope and an average grain size distribution. We chose to use this flow resistance equation as it has been shown to be suitable for flow having small relative submergence [*Ferguson*, 2010; *Rickenmann and Recking*, 2011] as is the case in the braided gravel bedded stream studied. Because of high lateral variability in hydraulics leading to potential bias when values are averaged over the cross section [*Ferguson*,

2003; *Nicholas*, 2000; *Paola*, 1996; *Recking*, 2013a], several homogeneous vertical panels were considered independently to compute locally averaged parameters as proposed by Bertoldi et al. (2009) or Nicholas et al. (2000) for braided morphology. This allowed us to estimate a local or average Shield parameter (dimensionless shear stress relative to a given grain size) considering the 84th percentile of the grain size distribution ($\tau_{84}{}^{*}$) in each cross-section and to compare this parameter with bedload transport rates (see Appendix A for details on the calculation of $\tau_{84}{}^{*}$).

4. RESULTS

4.1. OVERVIEW

Figure 3 shows the time-series of all the measurements conducted during the field campaign. Water discharge varies between 8 and 26 m^3 s^{-1} and exhibits daily peak discharge due to snowmelt, and sometimes due to rain events. The maximum instantaneous peak discharge measured corresponds to approximately a 2-year return period as calculated by the French hydrometric services (http://www.hydro.eaufrance.fr) based on 49 years of measurements. This suggests that our field campaign documents common flow conditions and exclude extreme events (5-year, 10-year and 20-year return period of 44, 56 and 68 m^3/s respectively). Indirect, seismic measurements also exhibit daily fluctuation, varying about three orders of magnitude, suggesting that the flow rate exerts a significant control on bedload transport in this river. The temporal seismic variability is also consistent with direct bedload sampling measurements.

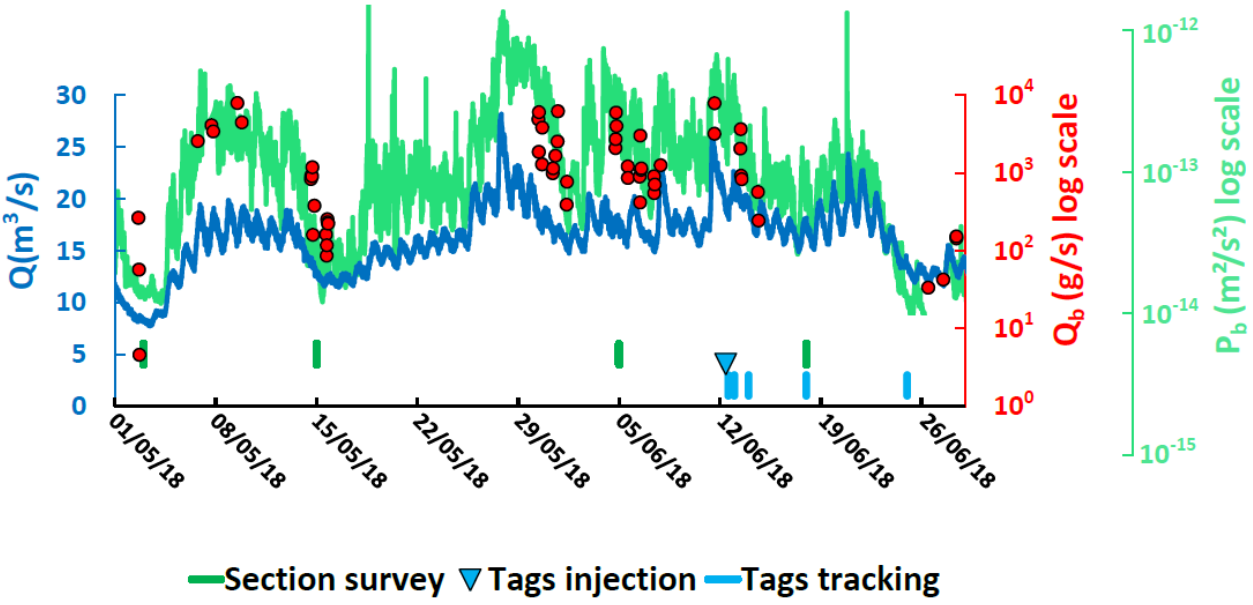

Figure 3: Time series of flow rate (Q, m3/s), seismic power at seismic1 (P_b, m^2/s^2) (20-80Hz) and direct bedload sampling measurements (Q_b, g/s). The dates of cross section survey, tag injection and tracking are indicated.

The main topographic and bed grain size distribution characteristics (detailed in the following sections) exhibit significant differences between the braided and the confined sections (Table 2). The braided sections have wider active widths, gentler slopes, and finer bed materials which suggests a more active morphology in this area.

	Slope (%)	Bed D_{50} range (mm)	Bed D_{84} range (mm)	Total active width range (m)
Braided sections (S1 to S4)	1.05	37-49	94-123	50-90
Confined section (S5)	1.2	110	303	12

Table 2: General river bed characteristics of the studied reach for braided sections (S1 to S4, located in Figure 2) and the confined section (S5). Bed D_{50} and D_{84} range correspond to the 50th and 84th percentiles of non-truncated Wolman counts performed in early May and late June in both channel sides and top bars (details can be found in supplementary material).

4.2. BEDLOAD DYNAMIC

Bedload transport rates range from 0.3 to 592 g s^{-1} m^{-1} (Figure 4) and are available as supplementary material. The general increase of unit bedload rate (q_b) with flow rate (Q) exhibits a power law with an exponent of 5.3 by fitting a log linear model. We observe a variability in bedload transport flux of one order of magnitude at a given flow rate, as is often found in gravel bedded streams [*Recking*, 2013b]. Part of this variability is time-dependent, as relatively larger transport rates occur at the beginning of the field campaign as confirmed by the resampling technique detailed in Appendix C.

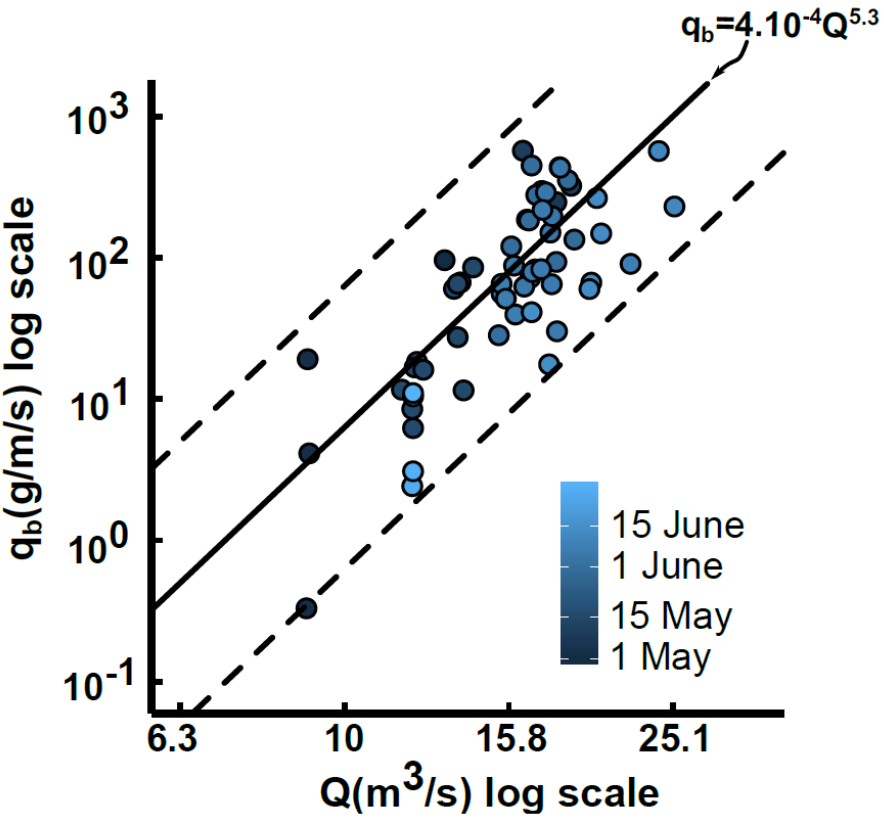

Figure 4: Sampled unit bedload transport rates measured at the gauging station (S5) as a function of flow rate for the whole field campaign. The black line is the best power law fit using all the data, dashed lines correspond to one order of magnitude around this best fit.

The average transported diameters are respectively 33 and 77 mm (n=17) for D_{50} and D_{84}, which is similar to the bed material sampled in the main channel of the braided sections, where D_{50} was between 28 and 43 mm and D_{84} between 63 and 123 mm, considering the start and the end of the campaign (Figure 5-a). These measurements

are available as supplementary material. On the opposite, the confined section has a much coarser bed (D_{50}=110 mm and D_{84}=303), which suggests that bedload samples at S5 do not come from a local bed mobilization but from material mobilized from the upstream braided sections. While the estimation of the coarsest transported diameter might be potentially underestimated due to the size of the sampler intake compare to bedload particles size, no significant trend is observed between the transported grain size and the flow rate even when only samples with small diameters are considered (Figure 5-b). The absence of such a relationship indicates a more or less equal mobility of bed material when delivered to the flow following local morphological changes such as bank failure or armor breakup.

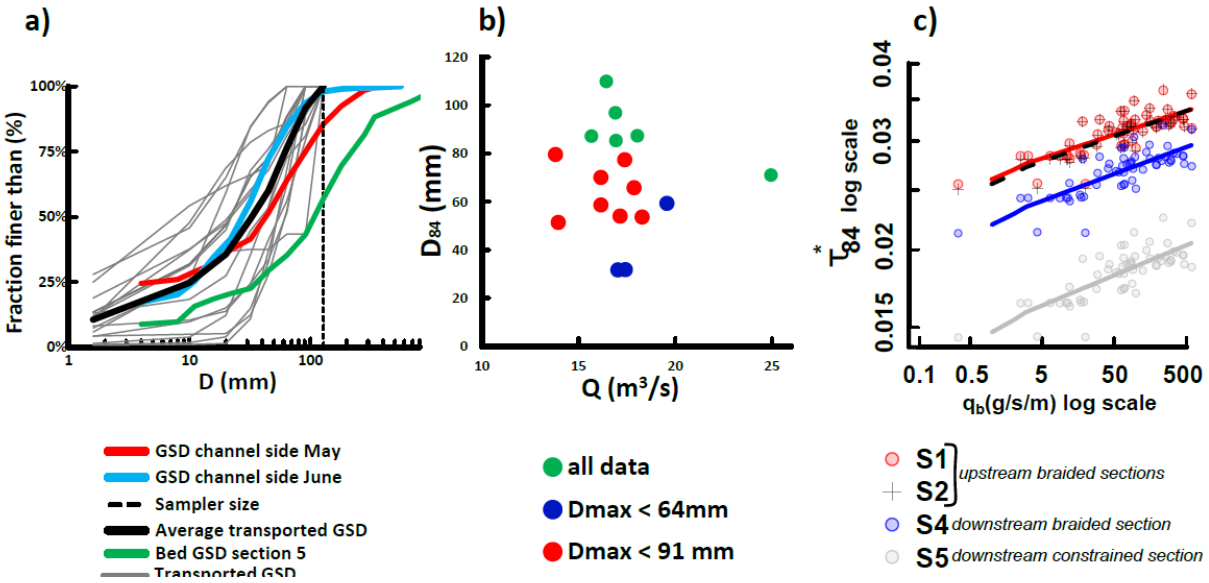

Figure 5: (a) River bed and transported grain size distributions. (b) 84th percentile of the transported diameter as a function of flow rate depending, points color indicates the range of maximum diameter sampled. (c) Shields number in the main active channel calculated considering four cross sections (beginning of the campaign, location in Figure 2) as a function of bedload fluxes measured.

For a given bedload transport rate, calculated bed related Shields numbers in the upstream cross sections of the braided reach (S1 and S2) are similar although slightly larger than the ones in the more downstream (S4) cross section (Figure 5-c). On the contrary, much lower Shields numbers for equivalent bedload transport rates is

observed in the narrow, paved and laterally confined section where bedload sampling were conducted (S5).

4.3. SEISMIC OBSERVATIONS

We observe that seismic power at *Seismic1* station is a power law function of flow discharge (Figure 6). Where grain size does not significantly vary with flow discharge (Figure 5), previous theory and laboratory experiments indicate that bedload-induced seismic power scales linearly with bedload flux (see Eq.2, Tsai *et al.* (2012) and Gimbert *et al*. (2019)), i.e. P_b scales with Q similarly than q_b does. Turbulent-flow-induced seismic power, however, is expected to scale with discharge to the power 7/5 [*Gimbert et al.*, 2016]. Best data fit with a power law model of our measurements gives a power law exponent of 3.9, which is significantly larger than the 7/5 exponent theoretically expected for seismic power associated to the turbulence of the flow. However this 3.9 exponent is significantly lower than the 5.3 exponent expected from the theory and lower than our previously inferred relationship between sediment transport flux and flow discharge (Figure 4). It is thus likely that a source other than turbulent flow generates significant ground seismic motion. This source is likely bedload, although we cannot yet conclude whether the observed discrepancy in P_b and q_b versus Q exponent between observations and theoretical expectations is due to turbulent flow or any other potential river source significantly contributing to seismic power or to theory not being applicable in such context.

We also observe a temporal trend in the P_b versus Q relationship with a decrease of the intercept along the two months highlighted by the two power laws fitted for the 10 first days of May and the 10 last days of June (Figure 6). Similar trend was previously observed at the seasonal scale in the Trisuli River in Nepal by Burtin *et al.* (2008), and at shorter timescales in various river settings [*Díaz et al.*, 2014; *Hsu et al.*, 2011; *Roth et al.*, 2016]. Such trend in seismic power versus flow discharge has often been interpreted as the result of a concomitant trend in bedload versus discharge. However, in these previous studies, no independent direct measurements allowed confirming such an interpretation. Our present observations provide such a confirmation, since the temporal

trend in P_b versus Q occurs concomitantly with the temporal shift in q_b and Q (Figure 4 and Figure 6). The decrease of the intercept through time could be indicative of a decrease in upstream sediment supply.

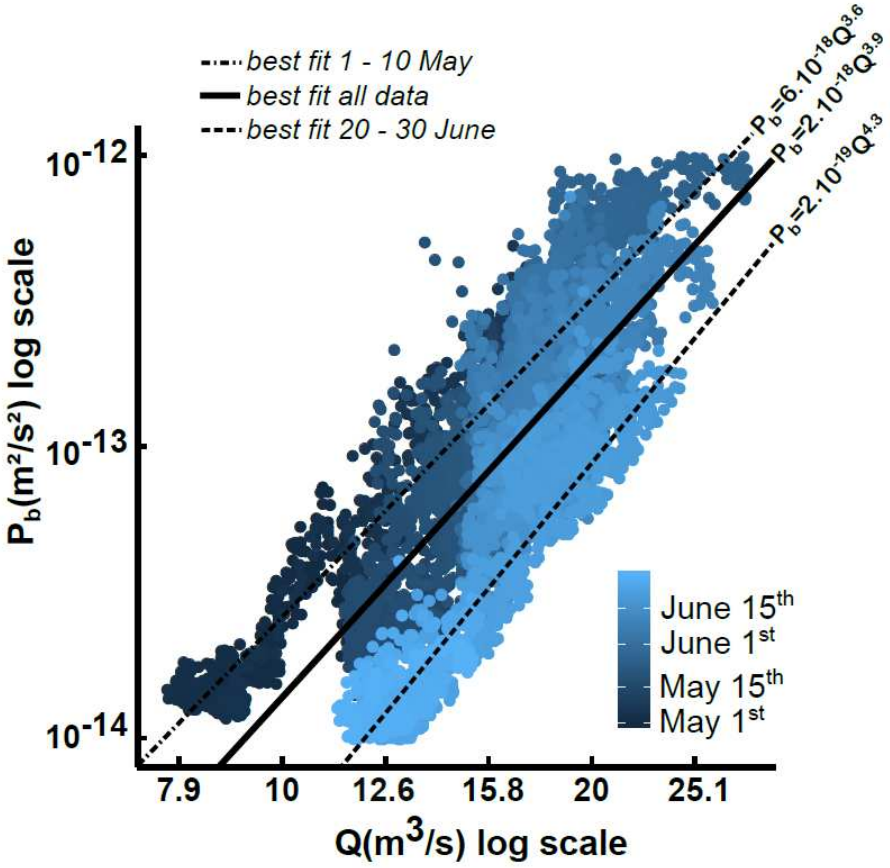

Figure 6: Seismic power at Seismic1 on a frequency range 20-80Hz as a function of the flow rate on a 10-minute basis. Best fit power laws are plotted for the start and the end of the campaign as well as for all the data.

The second seismic station tested on the Séveraisse reach, initially developed for debris flow monitoring (Seismic2 in Figure 2, which records with a 5-Hz frequency a proxy of the seismic energy integrated in the frequency band 0-80Hz) also shows a decrease with time of its geophone activity (Figure 7). Despite this signal cannot directly be compared to the conventionally used seismic sensor signal (their locations differ, the frequency range for which the signal power is calculated differs, etc.) and inverted into bedload flux using theoretical models, this decrease of geophone activity is consistent

with the decrease of bedload activity deduced from direct bedload sampling and the conventional seismic sensor measurements.

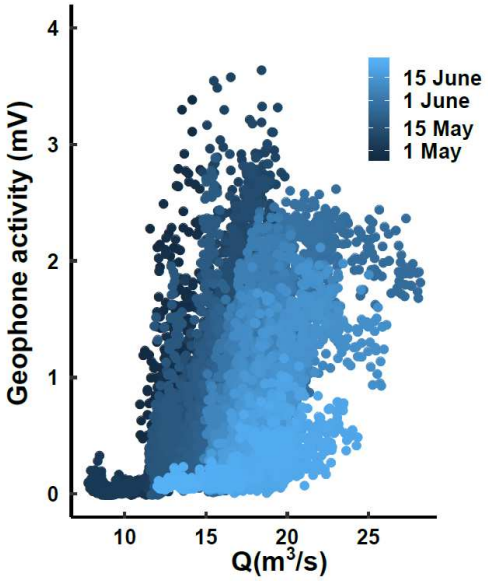

Figure 7: Low-cost geophone activity (Seismic2 in Figure 2) as a function of flow rate during the two-month field campaign.

4.4. BEDLOAD PARTICLE MOBILITY

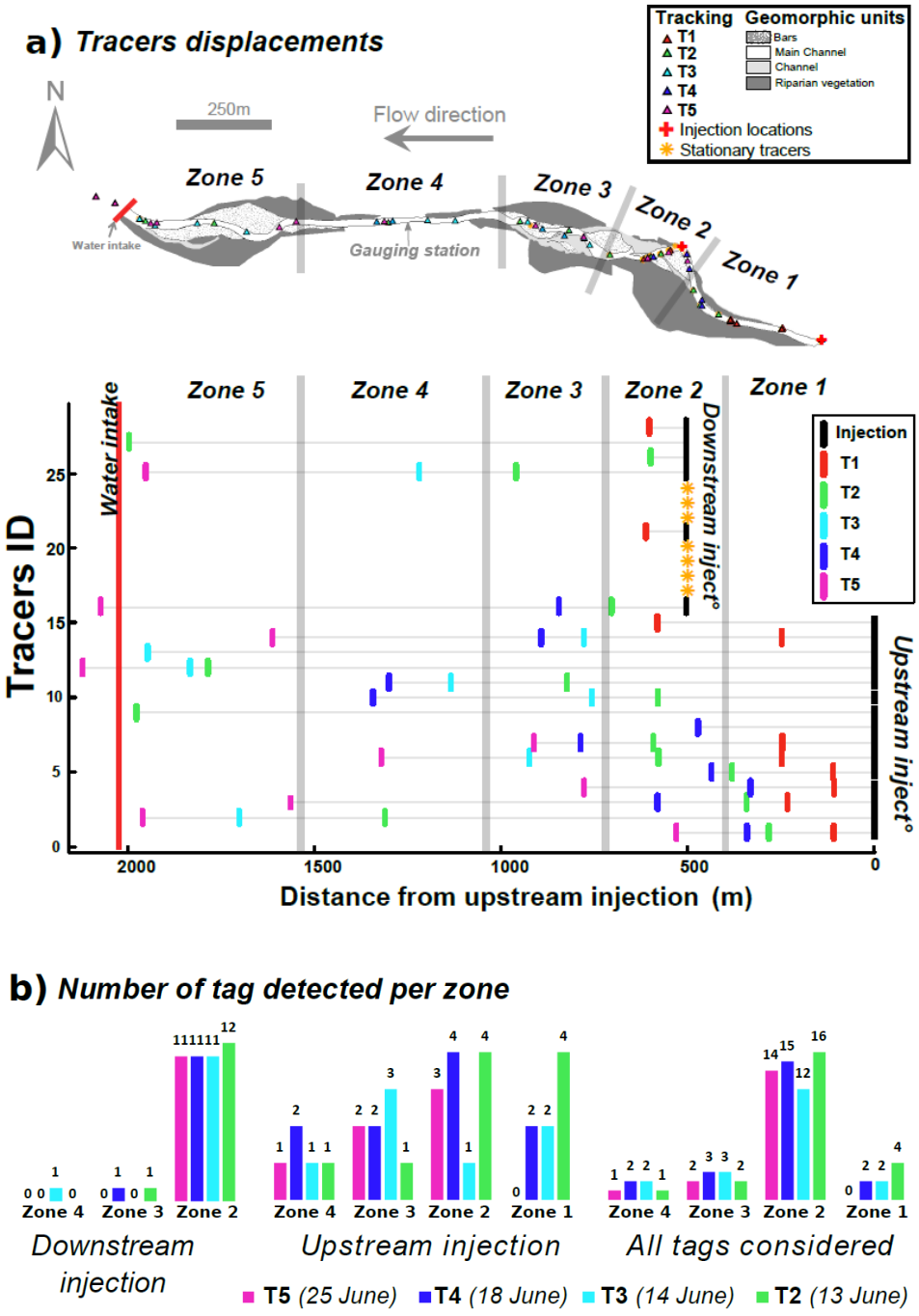

Figure 8: (a) Tracers displacements during the five tracking surveys (T1 to T5) following the injection. (b) Number of tags detected in each zone of the studied reach considering all tags or upstream and downstream injection separately. Note that the following tags were still found in Zone 2 on the 30th of august: 8, 15, 17, 19, 20, 21, 23, 24, 26, 28 and 29.

Pebble tracking surveys confirm the high bedload transport intensity during this field campaign. Following the tag tracers injection, most of them were retrieved when the whole reach was prospected thanks to their active UHF signal (return rate between 72% and 86%). This high recovery rate permits to be confident on the representativeness of these measurements. The pebbles were highly mobile with a maximum distance of nearly 2 km traveled over the course of one day (see T2, Figure 8). Thus, after the second day, several tags might have moved beyond the prospected zone and their travel distances or velocities cannot be observed. Assuming that the second full prospection (13th of June) is representative of the pebble dispersion (not too much tags downstream the prospected zone), a mean velocity can be estimated for the upstream and downstream injection point of respectively 27 and 13 meters per hour. These velocities can be compared to bedload fluxes obtained with direct sampling using the virtual velocity method [*Haschenburger and Church*, 1998]. Using the power law fitted between bedload rate and flow rate (Figure 4), a flux of 330 tons was estimated during the period corresponding to the two prospection dates (12/06 and 13/06) used to estimate virtual velocities. Assuming an active width range of 5-10 m and an apparent density of bed material of 2000 kg m^{-3} (corresponding to a porosity of nearly 25%), the active layer depth needed so that both independent bedload measurements are equal would range between 2 and 10cm. This range is consistent with values found in previous works, indicating that exchanges associated with bedload occur to a depth of $1D_{90}$ and do not exceed $2D_{90}$ [*DeVries*, 2002; *Hassan and Bradley*, 2017].

Moreover, during the prospection, no pebbles were found in secondary channels or on bars indicating that these coarse grains were mainly transported through the main channel. It was also observed that the number of tracked pebbles detected may depend on the zones (1 to 4) of the reach considered (Figure 8). It appears that pebbles transit through the narrow confined upstream and downstream parts of the reach (zone 1 and 4) more quickly than through the braided parts of the reach (zone 2 and 3). Considering all tags, almost half of them (14/29) were still at the entrance of the braided reach (zone 2) after the last prospection while only few tags were still detected in other zones. However, different behavior was observed depending on the injection point. 78% of the tags injected few meters upstream of zone 2 (downstream injection) stayed at the

entrance of the braided reach (zone 2) or traveled through the entire prospection zone. Conversely, a smaller proportion of tags injected from the upstream point (in the confined reach almost 500 meters upstream zone 2) stayed in zone 2. However, the entrance of the braided reach was still the zone in which most tags stayed until the end of the survey. It must also be highlighted that the entrance of the braided reach (zone 2) is only 200-meter-long compare to respectively 400, 400 and 500 meters for zone 1,3 and 4.

4.5. MORPHOLOGICAL CHANGES

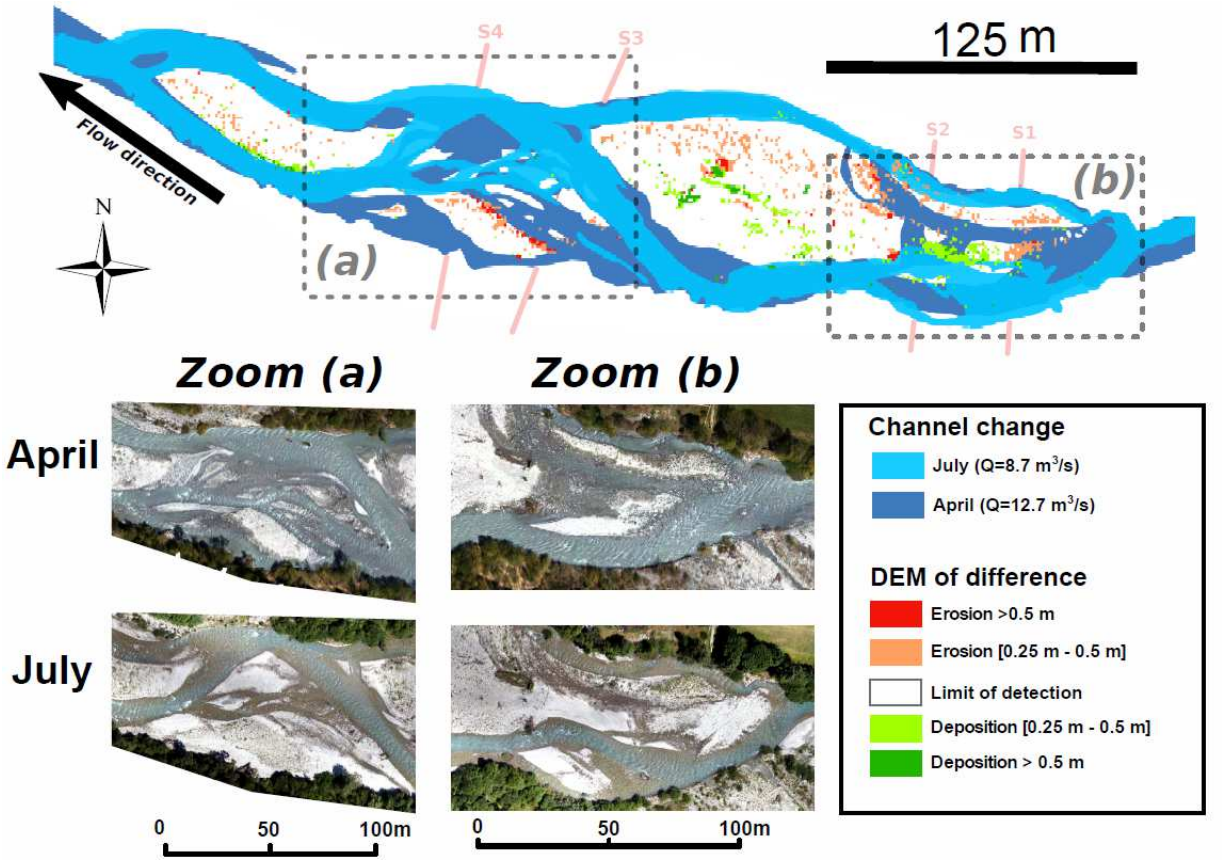

Figure 9: Diachronic analysis of the channels displacement between April and July using orthophotographs digitalisation and digital elevation model (DEM) of difference between April and july. Surveyed cross sections (S1 to S4) are indicated by red lines.

Orthophotographs, repeated topographic surveys, ground-based pictures show that the braided reach experienced significant planar and elevational changes during the study period (Figure 9, Figure 10 and Figure 11). First, the entrance and the middle part of the braided reach (respectively zone b and zone a in Figure 9) exhibit high braiding intensity with complex multi-channel flows leading to several confluences and bifurcations. These zones are particularely active with bars formation or banks and bars erosion. Second, the entrance of the braided reach experienced significant morphological changes, as shown in cross section surveys and ground-based pictures (Figure 10, Figure 11 a and b). Based on cross section surveys, net deposition was observed with bed aggradation

of locally more than one meter in this area (average depth change of respectively +11 cm and +13 cm for section 1 and 2). Morphological changes occurred from an incised channel configuration in May (one main channel on the left and one not well-connected secondary channel on the right) to a more distributed channel in June, associated with water being more evenly spread over the cross section (two main channels on the left and one active secondary channel on the right). Lateral channel migration took place near the entrance zone, amounting to 2.9 meters and 1.4 m of left bank erosion for section 1 and 2. Third, other cross sections (3 and 4) in the downstream active zone were more stable as no major bed elevation changes were detected (Figure 11-c and d) while bank erosion and lateral migration was significant for section 4 with almost 6 meters of right bank erosion. Lidar measurements on emerged top bars showed limited elevation changes for these zones. It indicates that underwater areas were the most active zones in this braided reach as suggested by the cross section measurements obtained using the topographic total station.

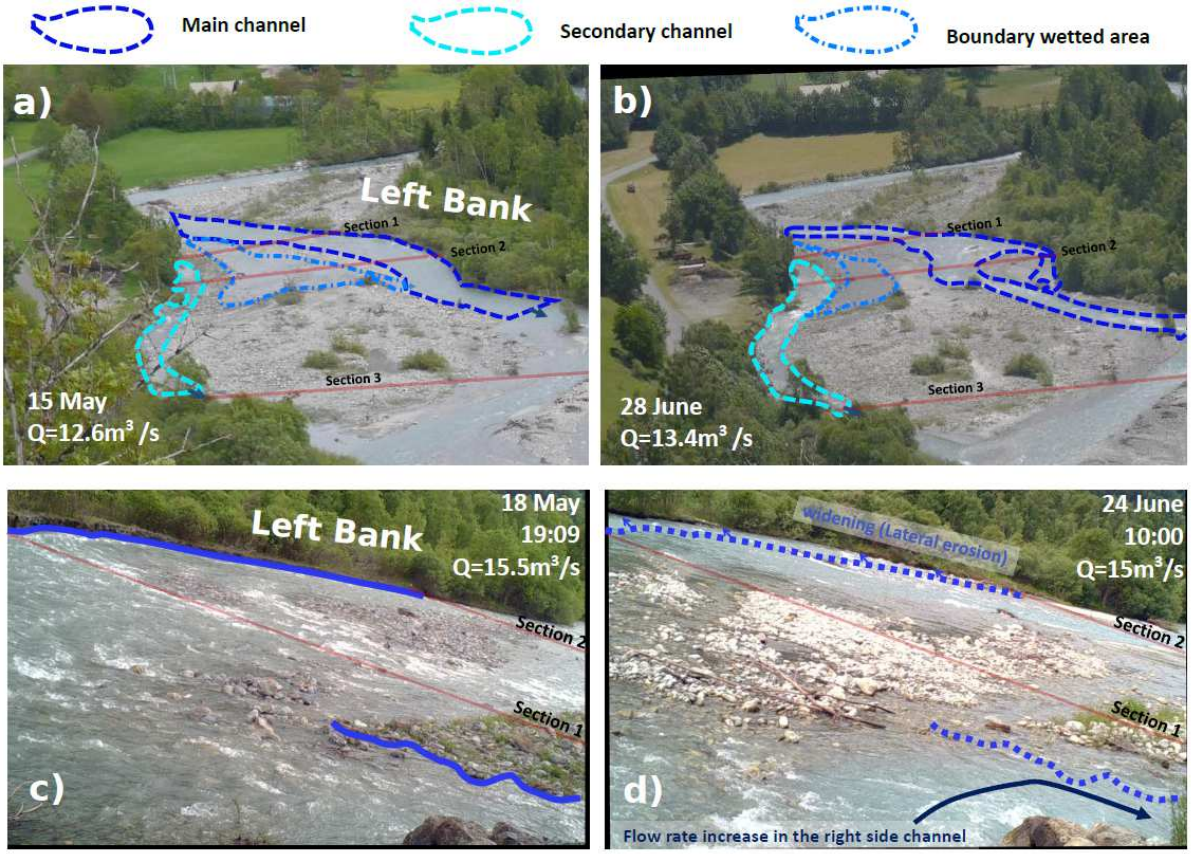

Figure 10: Morphological changes observed at the entrance of the downstream braided reach. Top view of the entrance of the downstream braided reach at the beginning (a) and at the end (b) of the campaign. View of the entrance of the downstream braided reach at the beginning (c) and at the end (d) of the campaign for the same discharge. Other ground-based pictures of the downstream part of the reach can be found in supplementary material.

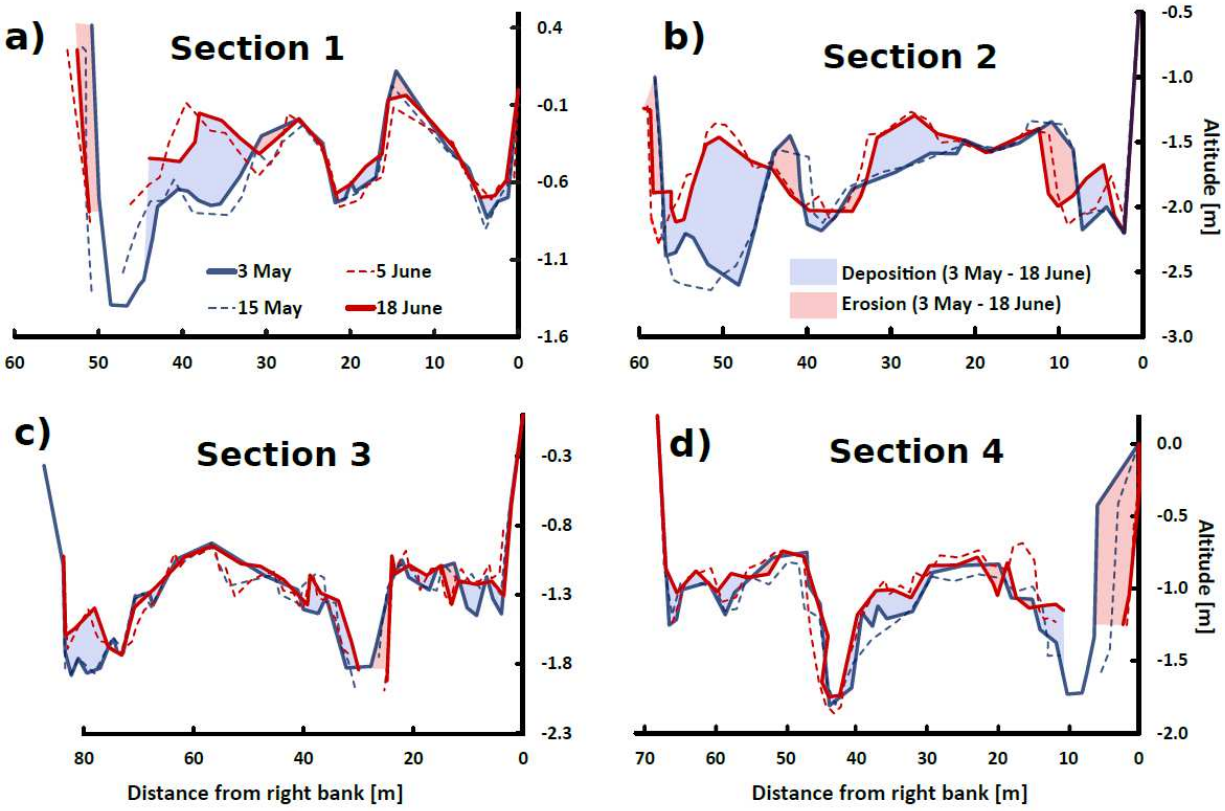

Figure 11: Topography evolution at the entrance of the downstream braided reach for section 1 (a), section 2 (b), section 3 (c) and section 4 (d).

Surface grain size analysis of the braided reach show a decrease in D_{50} and D_{84} from respectively 49mm and 123 mm at the beginning of the campaign to 37 and 94 mm at the end of the campaign (Figure 12). Top bars exhibited more or less constant coarse grain size distribution while much less fine particles (<10mm) were observed in June. Conversely, in the main channel, the fine fraction was constant while a decrease in coarse grain size was observed.

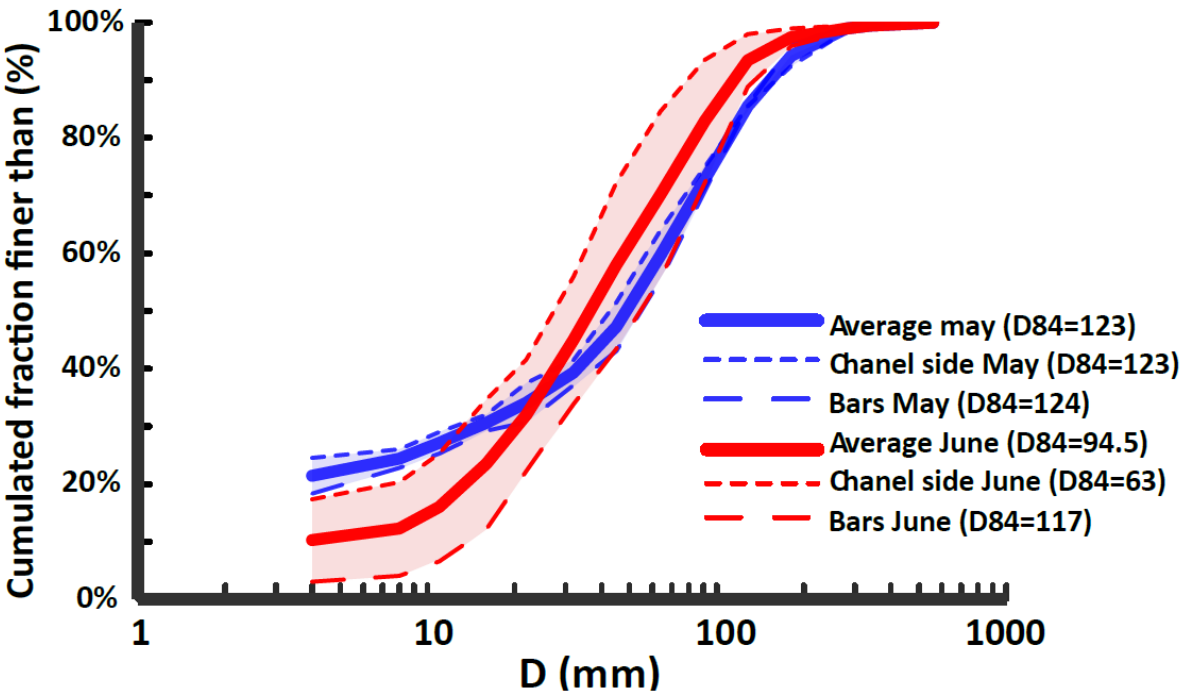

Figure 12: Surface grain size distribution of the studied reach at the begenning and the end of the field campaign, considering the main channel side and top bars.

4.5. HYDRAULIC CHANGES

The variability of transport capacity was computed by considering the morphological changes observed previously. The morphological changes observed in the cross section 2 lead to higher average shear stresses and average Shields numbers as calculated (for a given flow rate) in early May compared to late June (Figure 13-c), despite the smaller bed grain size in June (Figure 12). Local Shields number distributions ($\tau_{84}{}^{*}$, calculation detailed in Appendix A) also showed differences over the whole cross section due to morphological changes (Figure 13-a, Figure 13-b and Table 3). Shields numbers were more uniformly distributed around 0.025 (for Q=10m^3/s) in late June with fewer low and high values. A similar trend was observed at 20m^3/s discharge. The decrease of high-percentile Shields numbers during the season was consistent with a decrease in bedload rate for similar flow rates, as observed in Figure 4. This suggests that high-percentile Shields numbers control the bedload fluxes exported from such braided

reaches as observed in flume experiments by Bertoldi et al. (2009). It is also consistent with the fact that tracked pebbles were found only within the main active channel.

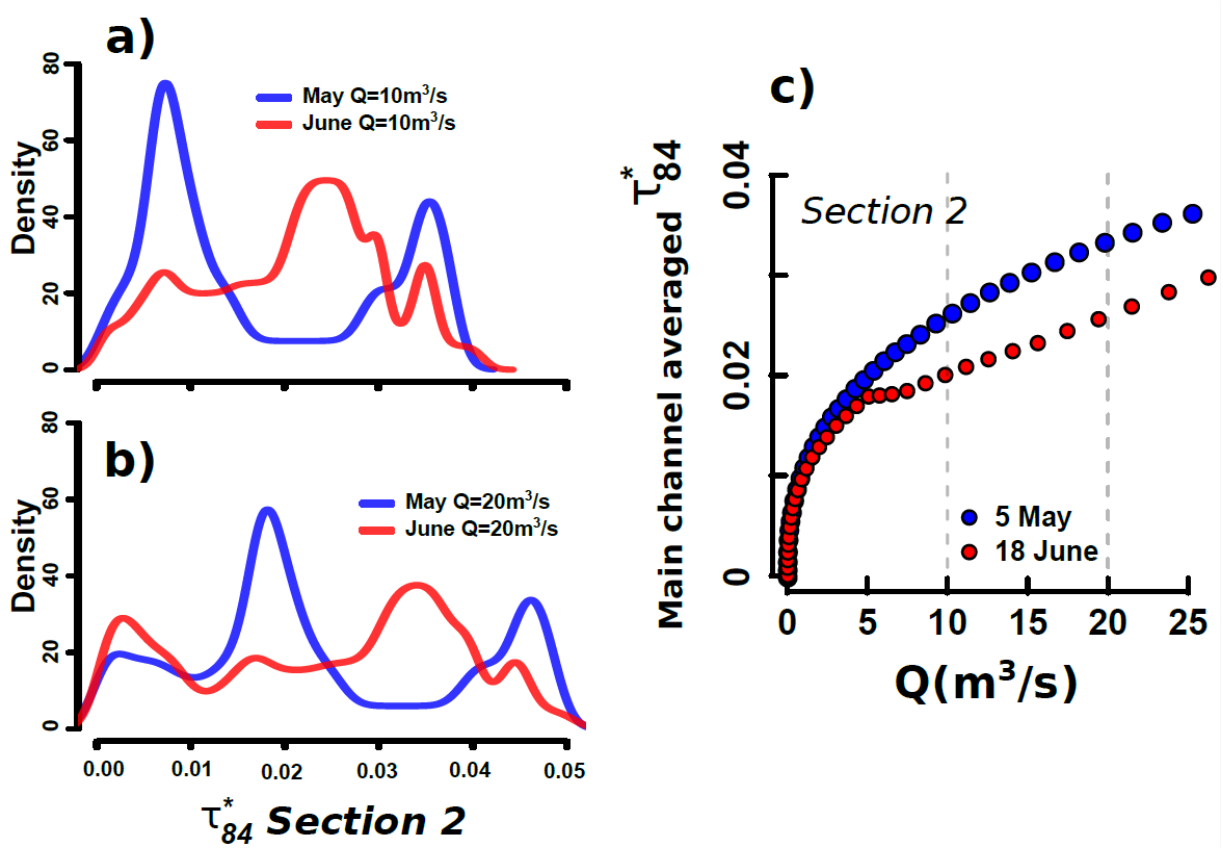

Figure 13: Probability density distribution of local Shield number calculated for a flow rate of (a) 10 m³/s and (b) 20 m³/s at the begenning and at the end of the campaign. (c) Averaged Shields number calculated in the main channel as a function of the flow rate, considering cross section 2 and grain size distribution at the beginning and at the end of the campaign. Discussion

5. DISCUSSION

5.1. ON THE VALUE OF COMBINING MULTIPLE FIELD TECHNIQUES

To quantify the interactions between bedload and morphology, both high spatial and temporal resolutions are required as bedload transport is highly variable at various time scales (instantaneous, event-based, or seasonal scale) and morphological changes have a large spatial extent. This field campaign on a particularly suitable site (high

predictable flow and sediment transport variability during 2 months, accessible riverbed, feasible direct sampling) shows that the combination of novel, continuous indirect measurements (seismics), direct field measurements (bedload sampling, cross section survey, pebble tracking), and drone-based and ground-based remote sensing imagery provides an informative set of observations on the dynamics of a complex braiding system. In other settings, such combination of multiple field techniques should be adapted to the local river system conditions. For instance, in large braided rivers (e.g. the Tagliamento, the Rees or the Sunwapta rivers) where direct sampling are not feasible (no confined sections), bedload fluxes could be estimated indirectly by using the morphological method [*Antoniazza et al.*, 2019; *Ashmore and Church*, 1998; *Lane et al.*, 1995; *Vericat et al.*, 2017] or the virtual velocity approach [*Haschenburger and Church*, 1998; *Liébault and Laronne*, 2008; *Mao et al.*, 2017]. In our case, the joint direct bedload measurements and seismic signals allowed us to detect unambiguous decrease through time over the two months period of the bedload activity which would have been difficult to conclude using only one of the two measurements. As direct measurements of bedload are time consuming and not always achievable, they are often sparse in time. Even though a rather high number of bedload direct measurement (60) could have been done during this field campaign given the good access facilities to the site and the presence of a field team on site, less measurements were available for example by the end of the June (Figure 4). The fact that the continuous seismic monitoring provided measurements at that period and showing the same trend, allowed us to be more confident on the decrease with time of the bedload activity. Conversely, even though seismic monitoring is continuous, it cannot easily be inverted to estimate bedload flux. It thus benefited from the comparison with direct measurements. Future studies (where bedload sampling is feasible) should focus on using direct sampling to better understand the seismic signal so that this type of data can be properly inverted into bedload flux.

Also, interesting perspectives (Figure 7) were observed concerning the use of the seismic sensor initially developed for debris flow monitoring (*Seismic2* station in Figure 2). This station (which records with a 5-Hz frequency a proxy of the seismic energy integrated in the frequency band 0-80Hz) detected the decrease with time of bedload activity (Figure 7). It suggests that this type of “low-cost” device requiring limited field

maintenance could be of interest when installing a monitoring network at the catchment scale to detect the temporal evolution of bedload in the different geomorphic units of the catchment. However, one must keep in mind that a proper comparison (by putting both sensors at the same location) with a conventional seismic device recording the full high frequency waveform continuously is needed to better characterize the geophone signal presented in Figure 7.

By combining complementary techniques such as pebble tracking, ground time-lapse cameras, direct cross section surveys, and drone imagery, we were able to quantify spatial morphological changes (bed mobility, lateral and vertical changes). Similarly to bedload measurements, we should stress that it would not have been possible to draw clear and robust conclusions by using only one of these techniques alone. Lidar data permitted to quantify elevation changes with a large spatial extent but were sparse in time (2 dates) and concerned only emerged bars excluding most changes in our case (Figure 9). Consequently, the repeated cross section surveys to quantify locally underwater elevation changes appeared to be essential as other remote measurements were not efficient in these zones considering our field campaign conditions: no signal return for Lidar, too high turbidity for any bathymetric estimation using SFM or colorimetry techniques as was done in Williams et al. (2014). They were also essential to estimate hydraulic parameters related to bedload transport. While ground-based camera is challenging to use as a quantitative measurement [*Benacchio et al.*, 2017] such technique was really useful to qualitatively confirm the other observations with a high temporal resolution. Adding information of pebble tracking, a dynamic measurement of morphology changes, permitted to analyze the longitudinal dynamic and the location of bedload transport in the reach. It confirmed that the main channel was the most active area which corroborates that average hydraulic parameters related to bedload transport should preferentially be calculated in that zone.

The virtual velocities obtained were also consistent with fluxes obtained with direct bedload sampling (realistic equivalent active layer values were estimated). Future studies using pebble tracking should carefully consider the injection point (injection in single channel sections vs injection in multiple channel sections; injection during high

flows directly in the flow vs tracers deposited at the top of the bed during low flows) as it could have a significant effect on the tags propagation as was observed in our study: virtual velocities were on average twice higher for tracers initially injected in a single channel section. Moreover, the use of active tracers with high detection ranges could help to better detect the high traveling distances and virtual velocities that are challenging to capture with previously use tracking techniques. The virtual velocities (13-27 m/h) and maximum displacements (~2km) observed were in the higher range of the 33 studies (passive techniques using painted, magnets or PIT tag tracers) reviewed by Vázquez-Tarrío et al. (2018). We also observed much higher virtual velocities associated with a given shield number than those observed in the Tagliamento and Brenta rivers by Mao et al. (2017) or those observed in Carnation Creek by Haschenburger and Church (1998). The previously mentioned data would suggest a maximum virtual velocity of 4 m/h much lower than the 13-27 m/h observed in our case.

5.2. INTERACTION OF BRAIDED RIVER BED MORPHOLOGY WITH BEDLOAD FLUXES

The whole set of results acquired during the field campaign suggests that bedload and morphology are co-evolving during the two months melting season. In this period, a significant decrease in the bedload rate for a given discharge was observed with both direct sampling and indirect seismic measurements. Simultaneously, the braided bed morphology evolved from an incised to a more homogeneous river bed configuration. Similar temporal dynamic in braided rivers having a nival flow regime was reported by Warburton (1994) in the Bas Glacier d'Arolla or more recently by Middleton et al. (2019) in the Sunwapta river. The latter observed that most planimetric changes (related to bedload fluxes) occurred during the first high flow period of the melting season even though equivalent flows occurred later in the season (two consecutive years). This strong link between bedload and morphology observed in the Séveraisse river confirms previous flume studies relating bedload fluxes to volumetric, planimetric and active width changes [*Bertoldi et al.*, 2009a; *Middleton et al.*, 2019; *Peirce et al.*, 2018] . It is also consistent with field observations relating sediment supply and braided morphology

changes at various time and spatial scales [*Bakker et al.*, 2019; *Lane et al.*, 1996; *Liebault et al.*, 2013; *Pryor et al.*, 2011].

In the studied reach, aggradation caused a decrease in flow depth and a subsequent decrease of the highest percentiles of bed related Shields numbers for a given flow rate. Simultaneously, a decrease of bedload activity was observed. These simultaneous decreases suggest that bedload transport occurs mainly in concentrated zones, which is consistent with previous flume and field observations. For instance, using ADCP data in the Rees river, Williams et al. (2015) observed that the apparent velocities of bedload were concentrated in narrow zones of the main channel. Also, numerical [*Antoniazza et al.*, 2019; *Williams et al.*, 2013] and small scale modeling [*Egozi and Ashmore*, 2008] of braided rivers showed that only few channels (typically 1 or 2) exhibit high shear stresses and are actively transporting bed material despite there are several other wetted channels. This transport activity of only few channels is also confirmed in our study by the fact that during the a-UHF tags prospection, no pebbles were found in secondary channels or on bars indicating that coarse bedload particles were transported predominantly in the main channel. This predominant transport path was also reported by Liebault et al. (2012) in a braided river from the southern Alps. The mobility of tracers initially deployed in the low-flow channel was 15 to 30 times higher than the mobility of tracers deployed on bars. All of these observations suggest that average hydraulic parameters controlling bedload transport (Shield number, dimensionless stream power) should preferentially be calculated in that zone rather than over the whole width of a given reach as suggested by previous studies [*Bertoldi et al.*, 2009a; *Nicholas*, 2000].

Considering interactions between bedload and braided morphology at a broader scale, the confined-unconfined (braided) sequence presented in this study can be of interest for better understanding the transfer of bed material in mountainous systems. As shown in Figure 1 for the Séveraisse, Alpine catchments are often characterized by a succession of confined (due to gorges, narrow valley or torrential fans) and unconfined reaches where braiding often develops. For instance, such typical sequence of fluvial styles is reported by Arnaud-Fassetta et al. (2005) for the Guil river. In that context of successive braiding and confined sections, our study suggests that bedload rate and

morphological changes are more closely related in the braiding sections (S1, S2, S4) than in the confined ones (S5), in which bedload fluxes may not result from local bed mobilization. The following observations support this conclusion:

(i) No morphological changes were observed in the confined section while large changes were observed in the braiding one,
(ii) Tracked pebbles resided longer in the braiding section as compared to the confined one,
(iii) The average transported grain size distribution was similar to the bed grain size distribution found in the main channel side of the braided reach while the confined section had a much coarser bed,
(iv) Much lower Shields values for a given bedload rate were determined for the confined section compare to the alluvial ones,

Figure 14 shows a conceptual scheme, linking bedload and bed morphology in rivers with alternatively unconfined and confined sections. Alluvial reaches have bed morphology that may respond rapidly, through flow width, grain size distribution, etc., to local hydraulic forcing and upstream bedload fluxes. Such reaches could thus buffer upstream bedload fluxes and can be considered a source of sediment for downstream reaches: a strong link exists between morphological changes and bedload fluxes (structural bedload, transport capacity limited). On the contrary, bed morphology in confined reaches cannot adapt to local hydraulics and upstream bedload forcing under most conditions (extreme events excluded): upstream bedload fluxes are efficiently transferred without bed morphological changes according to the travelling bedload concept (supply limited) proposed for steep torrents that are highly connected to hillslope sources [*Piton and Recking*, 2017]. This has important implications for the choice of cross section where bedload calculations should preferentially be performed as discussed in the next section.

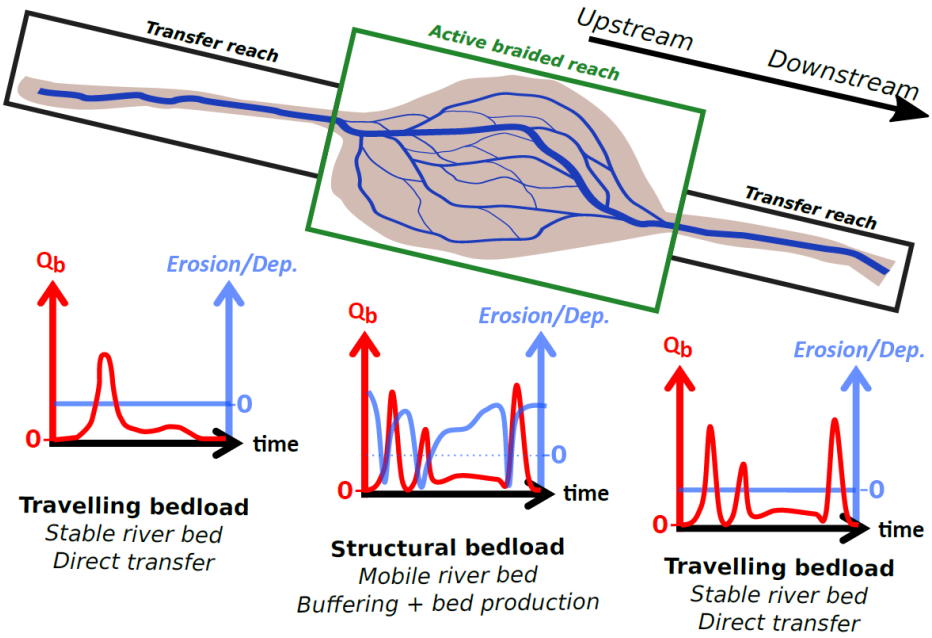

Figure 14: Conceptual diagram illustrating the influence of braiding on bedload transfer in alternating confined (transfer) and unconfined (alluvial) reaches typically found in Alpine streams. The transfer reaches are for most floods non-active in terms of morphology and can efficiently transfer bedload material from upstream (supply limited). There is no relation between bedload fluxes and bed morphology changes. The alluvial reaches (here braiding) can adapt their morphology to hydraulics and upstream sediment fluxes resulting in a strong relation between morphological changes and bedload exported downstream (transport capacity limited). "Q_b" denotes bedload fluxes; "Erosion/Dep." denotes erosion and deposition processes leading to morphological changes.

5.3. IMPLICATIONS FOR REACH-AVERAGED BEDLOAD MODELING

A noticeable interest of the complete data set acquired during this study is that it allows to build and run physically based and fully distributed numerical models to go further in the understanding of the bedload and morphology interactions and to test assumptions about the drivers of these interactions. This analysis will be conducted in the near future. Nevertheless, we should stress that our results also have general and immediate implications for the estimation of bedload rates in systems with alternating confined and unconfined sections for which direct bedload measurements are scarce. A key consideration is to choose where bedload calculation should be made to estimate bedload transport [*Recking et al.*, 2016] as confirmed by the variability of Shields number associated with a given measured bedload transport rate (Figure 5-c). Because

bedload and flow measurements were performed in the confined reach, it would have been logical to perform bedload calculation there. However, as discussed previously, bedload transport is better related to morphodynamics in the braided sections than in the confined sampling cross section S5. We thus applied in both the braided and confined sections the Recking bedload formula (presented in Appendix B) which is a relation between average Shield parameters and bedload transport rate (calibrated and validated on a large field dataset). Predictions were significantly improved when considering alluvial sections (S1, S2 and S4) compared to the confined and paved one (S5) (Figure 15) which is consistent with a limited production of bed material in the transfer reach compared to in the studied upstream braiding reach. The seasonal variability of the cross section and grain size distribution was considered for cross section 2. This led to small differences in term of predictions, compare to spatial differences due to the choice of cross section. This shows that applying bedload formula in such system should preferably be done in alluvial, morphodynamically active zones.

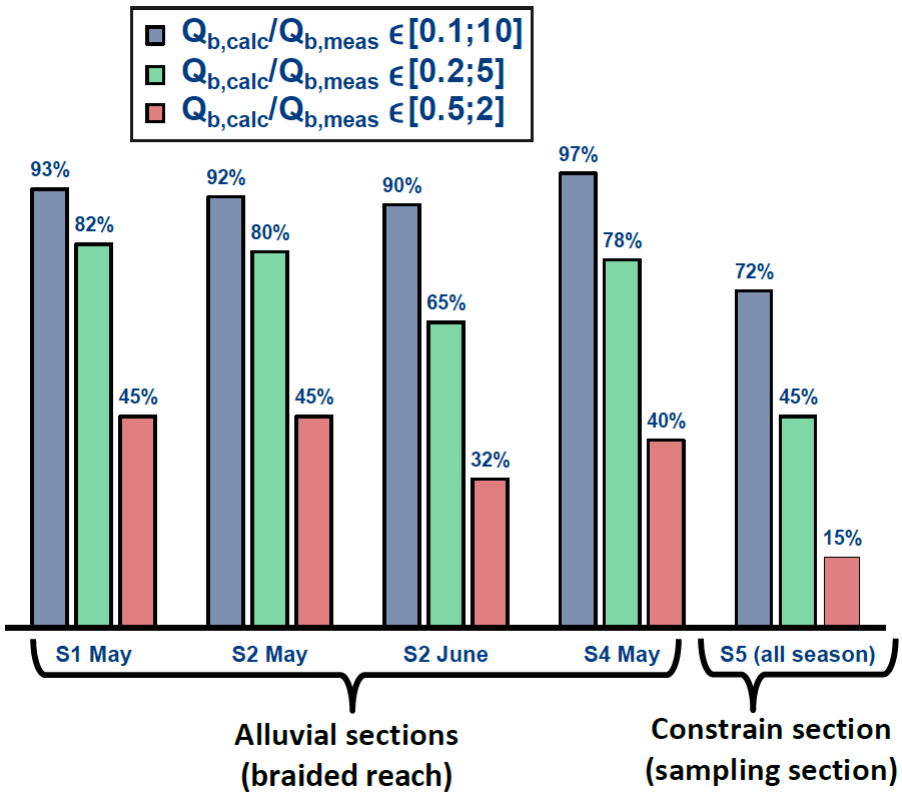

Figure 15: Predictions obtained with the Recking bedload formula depending on the cross section and date considered. To quantify the goodness of predictions, we calculated the percentages of ratios $Q_{b,\ calculated}/Q_{b,\ measured}$ that fell in the ranges [0.1-10], [0.2-5] and [0.5-2]. S1, S2 and S4 correspond to alluvial cross sections (in the braided reach) while S5 is the cross section where bedload fluxes were measured (confined and paved reach).

6. CONCLUSION

In this paper we analyze the relation between bedload transport and morphodynamic in a typical Alpine braided river by combining multi-physical measurements. We show that such approach combining both traditional direct measurements with novel indirect techniques permits a much deeper understanding of the physical processes often difficult to capture in the field with a single instrument. This study also highlights the interest to measure simultaneously bedload transport processes and river bed morphology changes. This is particularly relevant in braided river: strong interactions were observed between bedload transport and morphodynamics on the study site. These detailed observations confirm flume-derived hypothesizes stating that bedload particles in braided rivers are mostly transported in concentrated zones where shear stresses are high. Our observations showing that aggradationnal or degradationnal phases exert a significant control on bedload fluxes exported downstream are also in line with longer-term field observations. Finally, these results have important implications for modeling bedload in successive confined-braiding rivers typically found in mountainous environments.

While consistent observations were made in this study, braided rivers morphodynamic and bedload transport stay highly complex processes. For this reason, we think that future research should continue to combine such a large panel of techniques that needs to be designed according to specific conditions of the study area. In the case of the Séveraisse river, this could consist of inverting the seismic signal by using direct sampling or combining high-frequency imagery, pebble tracking, and a seismic array to localize with a high temporal resolution bedload transport path and intensity.

7. NOTATIONS

The following symbols are used in this paper.

D_{50}	Sediment diameter of the bed such that 50% of the mixture is finer $[m]$
D_{84}	Sediment diameter of the bed such that 84% of the mixture is finer $[m]$
D	Sediment diameter $[m]$
τ^*	Shields number: dimensionless shear stress [-]
τ_{84}^*	Shields number for D_{84} [-]
τ_m^*	Dimensionless transition parameter between partial and full mobility [-]
Q	Water discharge $[m^3/s]$
U	Mean water velocity over the section $[m/s]$
u^*	Friction velocity [m/s]
W	Channel bed width $[m]$
S	Channel bed slope $[m/m]$
ρ	Water density $[kg/m^3]$
ρ_s	Sediment density $[kg/m^3]$
s	Relative density of sediment [-]
g	Gravitational acceleration $[m/s^2]$
d	Mean water depth $[m]$
q	Unit water discharge $[m^3/s/m]$
Q_b	Bedload $[kg/s]$
q_b	Unit bedload $[kg/s/m]$
$q_b{}^*$	Dimensionless bedload [-]

P_b	Seismic power [m²/s²]
L_t	Cross section width [m]
L_i	Width considered representative for the sampling point I [m]
L_e	Sampler width [m]
$Q_{be\,i}$	Bedload rate for each sample [g/s]

8. ACKNOWLEDGMENTS AND DATA

This project was founded by IRSTEA, Eléctricité de France and the ANR grant 17-CE01-0008-01. Data supporting the content of this paper as well as other bedload sampling data taken from an upstream bridge (not presented in this paper) are available in the supplementary material and in a Mendeley data repository. More details can also be obtained by contacting IRSTEA (C. Misset or A. Recking). The authors are grateful to D. Vázquez-Tarrío, E. Gronlier, J. Paloucek and F. Bonazzi who helped for the field measurements; E. Mermin, F. Ousset and P. Tardif who helped to perform the drone flight.

9. REFERENCES

Antoniazza, G., M. Bakker, and S. N. Lane (2019), Revisiting the morphological method in two-dimensions to quantify bed-material transport in braided rivers, *Earth Surface Processes and Landforms*, doi:10.1002/esp.4633.

Arnaud-Fassetta, G., E. Cossart, and M. Fort (2005), Hydro-geomorphic hazards and impact of man-made structures during the catastrophic flood of June 2000 in the Upper Guil catchment (Queyras, Southern French Alps), *Geomorphology*, *66*(1-4), 41-67, doi:10.1016/j.geomorph.2004.03.014.

Ashmore, P., Bertoldi, and J. T. Gardner (2011), Active width of gravel-bed braided rivers, *Earth Surface Processes and Landforms*, *36*(11), 1510-1521, doi:10.1002/esp.2182.

Ashmore, P., and M. Church (1998), Sediment transport and river morphology: a paradigm for study., *Gravel-bed Rivers in the Environment*, *Hey RD, Bathurst JC, Thorne CR (eds). Wiley: Chichester.*, 115–148.

Ashmore, P. E. (1982), Laboratory Modeling of Gravel Braided-Stream Morphology, *Earth Surface Processes and Landforms*, *7*(3), 201-225, doi:0197-9337/82/030201-25$02.50.

Ashmore, P. E. (1988), Bed-Load Transport in Braided Gravel-Bed Stream Models, *Earth Surface Processes and Landforms*, *13*(8), 677-695, doi:DOI 10.1002/esp.3290130803.

Ashmore, P. E. (1991), How do gravel-bed rivers braid?, *Canadian Journal of Earth Sciences*, *28*(3), 326-341, doi:10.1139/e91-030.

Bakker, M., G. Antoniazza, E. Odermatt, and S. N. Lane (2019), Morphological Response of an Alpine Braided Reach to Sediment-Laden Flow Events, *Journal of Geophysical Research: Earth Surface*, doi:10.1029/2018jf004811.

Bakker, M., and S. N. Lane (2017), Archival photogrammetric analysis of river-floodplain systems using Structure from Motion (SfM) methods, *Earth Surface Processes and Landforms*, *42*(8), 1274-1286, doi:10.1002/esp.4085.

Bel, C., F. Liébault, O. Navratil, N. Eckert, H. Bellot, F. Fontaine, and D. Laigle (2017), Rainfall control of debris-flow triggering in the Réal Torrent, Southern French Prealps, *Geomorphology*, *291*, 17-32, doi:10.1016/j.geomorph.2016.04.004.

Benacchio, V., H. Piegay, T. Buffin-Belanger, and L. Vaudor (2017), A new methodology for monitoring wood fluxes in rivers using a ground camera: Potential and limits, *Geomorphology*, *279*, 44-58, doi:10.1016/j.geomorph.2016.07.019.

Bertoldi, W., P. Ashmore, and M. Tubino (2009a), A method for estimating the mean bed load flux in braided rivers, *Geomorphology*, *103*(3), 330-340, doi:10.1016/j.geomorph.2008.06.014.

Bertoldi, W., A. Gurnell, N. Surian, K. Tockner, L. Zanoni, L. Ziliani, and G. Zolezzi (2009b), Understanding reference processes: linkages between river flows, sediment dynamics and vegetated landforms along the Tagliamento River, Italy, *River Research and Applications*, *25*(5), 501-516, doi:10.1002/rra.1233.

Bertoldi, W., A. M. Gurnell, and N. A. Drake (2011), The topographic signature of vegetation development along a braided river: Results of a combined analysis of airborne lidar, color air photographs, and ground measurements, *Water Resources Research*, *47*(6), doi:10.1029/2010wr010319.

Burtin, A., L. Bollinger, J. Vergne, R. Cattin, and J. L. Nabelek (2008), Spectral analysis of seismic noise induced by rivers: A new tool to monitor spatiotemporal changes in stream hydrodynamics, *J Geophys Res-Sol Ea*, *113*(B5), doi:Artn B05301 10.1029/2007jb005034.

Burtin, A., R. Cattin, L. Bollinger, J. Vergne, P. Steer, A. Robert, N. Findling, and C. Tiberi (2011), Towards the hydrologic and bed load monitoring from high-frequency seismic noise in a braided river: The “torrent de St Pierre”, French Alps, *Journal of Hydrology*, *408*(1-2), 43-53, doi:10.1016/j.jhydrol.2011.07.014.

Cassel, M., T. Dépret, and H. Piégay (2017a), Assessment of a new solution for tracking pebbles in rivers based on active RFID, *Earth Surf. Process. Landforms*, *42*, 1938–1951, doi:10.1002/esp.4152.

Cassel, M., H. Piégay, and J. Lavé (2017b), Effects of transport and insertion of radio frequency identification (RFID) transponders on resistance and shape of natural and synthetic pebbles: applications for riverine and coastal bedload tracking, *Earth Surface Processes and Landforms*, *42*(3), 399-413, doi:10.1002/esp.3989.

Chapuis, M., S. Dufour, M. Provansal, B. Couvert, and M. de Linares (2015), Coupling channel evolution monitoring and RFID tracking in a large, wandering, gravel-bed river: Insights into sediment routing on geomorphic continuity through a riffle–pool sequence, *Geomorphology*, *231*, 258-269, doi:10.1016/j.geomorph.2014.12.013.

Cook, K. L., C. Andermann, F. Gimbert, B. R. Adhikari, and N. Hovius (2018), Glacial lake outburst floods as drivers of fluvial erosion in the Himalaya, *Science*, *362*(6410), 53-57, doi:10.1126/science.aat4981.

DeVries, P. (2002), Bedload layer thickness and disturbance depth in gravel bed streams, *J Hydraul Eng-Asce*, *128*(11), 983-991, doi:10.1061/(Asce)0733-9429(2002)128:11(983).

Díaz, J., M. Ruíz, L. Crescentini, A. Amoruso, and J. Gallart (2014), Seismic monitoring of an Alpine mountain river, *Journal of Geophysical Research: Solid Earth*, *119*(4), 3276-3289, doi:10.1002/2014jb010955.

Eaton, B. C., R. G. Millar, and S. Davidson (2010), Channel patterns: Braided, anabranching, and single-thread, *Geomorphology*, *120*(3-4), 353-364, doi:10.1016/j.geomorph.2010.04.010.

Egozi, R., and P. Ashmore (2008), Defining and measuring braiding intensity, *Earth Surface Processes and Landforms*, *33*(14), 2121-2138, doi:10.1002/esp.1658.

Ferguson, R. (2007), Flow resistance equations for gravel- and boulder-bed streams, *Water Resources Research*, *43*(5), doi:Artn W05427 10.1029/2006wr005422.

Ferguson, R. (2010), Time to abandon the Manning equation?, *Earth Surface Processes and Landforms*, *35*(15), 1873-1876, doi:10.1002/esp.2091.

Ferguson, R. I. (2003), The missing dimension: effects of lateral variation on 1-D calculations of fluvial bedload transport, *Geomorphology*, *56*(1-2), 1-14, doi:10.1016/S0169-555x(03)00042-4.

Gimbert, F., B. M. Fuller, M. P. Lamb, V. C. Tsai, and J. P. L. Johnson (2019), Particle transport mechanics and induced seismic noise in steep flume experiments with accelerometer-embedded tracers, *Earth Surface Processes and Landforms*, *44*(1), 219-241, doi:10.1002/esp.4495.

Gimbert, F., V. C. Tsai, J. M. Amundson, T. C. Bartholomaus, and J. I. Walter (2016), Subseasonal changes observed in subglacial channel pressure, size, and sediment transport, *Geophysical Research Letters*, *43*(8), 3786-3794, doi:10.1002/2016gl068337.

Gimbert, F., V. C. Tsai, and M. P. Lamb (2014), A physical model for seismic noise generation by turbulent flow in rivers, *Journal of Geophysical Research: Earth Surface*, *119*(10), 2209-2238, doi:10.1002/2014jf003201.

Gomez, B., R. L. Naff, and D. W. Hubbell (1989), Temporal variations in bedload transport rates associated with the migration of bedforms, *Earth Surface Processes and Landforms*, *14*(2), 135-156, doi:10.1002/esp.3290140205.

Gran, K., and C. Paola (2001), Riparian vegetation controls on braided stream dynamics, *Water Resources Research*, *37*(12), 3275-3283, doi:Doi 10.1029/2000wr000203.

Gray, J. R., J. B. Laronne, and J. D. G. Marr (2010), Bedload-surrogate monitoring technologies: U.S. Geological Survey Scientific Investigations Report 2010–5091, 37 p.,*Rep.*

Haschenburger, J. K., and M. Church (1998), Bed material transport estimated from the virtual velocity of sediment, *Earth Surface Processes and Landforms*, *23*(9), 791-808, doi:Doi 10.1002/(Sici)1096-9837(199809)23:9<791::Aid-Esp888>3.0.Co;2-X.

Hassan, M. A., and D. N. Bradley (2017), *Geomorphic Controls on Tracer Particle Dispersion in Gravel-Bed Rivers*, doi:10.1002/9781118971437.ch6

Helsen, M. M., P. J. M. Koop, and H. Van Steijn (2002), Magnitude-frequency relationship for debris flows on the fan of the Chalance torrent, Valgaudemar (French Alps), *Earth Surface Processes and Landforms*, *27*(12), 1299-1307, doi:10.1002/esp.412.

Hoey, T. (1992), Temporal Variations in Bedload Transport Rates and Sediment Storage in Gravel-Bed Rivers, *Progress in Physical Geography*, *16*(3), 319-338, doi:Doi 10.1177/030913339201600303.

Hsu, L., N. J. Finnegan, and E. E. Brodsky (2011), A seismic signature of river bedload transport during storm events, *Geophysical Research Letters*, *38*(13), n/a-n/a, doi:10.1029/2011gl047759.

Lallias-Tacon, S., F. Liebault, and H. Piegay (2014), Step by step error assessment in braided river sediment budget using airborne LiDAR data, *Geomorphology*, *214*, 307-323, doi:10.1016/j.geomorph.2014.02.014.

Lane, S. N., K. S. Richards, and J. H. Chandler (1995), Morphological Estimation of the Time-Integrated Bed-Load Transport Rate, *Water Resources Research*, *31*(3), 761-772, doi:Doi 10.1029/94wr01726.

Lane, S. N., K. S. Richards, and J. H. Chandler (1996), Discharge and sediment supply controls on erosion and deposition in a dynamic alluvial channel, *Geomorphology*, *15*(1), 1-15, doi:Doi 10.1016/0169-555x(95)00113-J.

Lane, S. N., R. M. Westaway, and D. M. Hicks (2003), Estimation of erosion and deposition volumes in a large, gravel-bed, braided river using synoptic remote sensing, *Earth Surface Processes and Landforms*, *28*(3), 249-271, doi:10.1002/esp.483.

Liébault, F., H. Bellot, M. Chapuis, S. Klotz, and M. Deschâtres (2012), Bedload tracing in a high-sediment-load mountain stream, *Earth Surface Processes and Landforms*, *37*(4), 385-399, doi:10.1002/esp.2245.

Liebault, F., S. Lallias-Tacon, M. Cassel, and N. Talaska (2013), Long Profile Responses of Alpine Braided Rivers in Se France, *River Research and Applications*, *29*(10), 1253-1266, doi:10.1002/rra.2615.

Liébault, F., and J. B. Laronne (2008), Evaluation of bedload yield in gravel-bed rivers using scour chains and painted tracers: the case of the Esconavette Torrent (Southern French Prealps), *Geodinamica Acta*, *21*(1-2), 23-34, doi:10.3166/ga.21.23-34.

Lisle, T. E., and M. Church (2002), Sediment transport-storage relations for degrading, gravel bed channels, *Water Resources Research*, *38*(11), 1-1-1-14, doi:10.1029/2001wr001086.

Luchi, R., Bertoldi, G. Zolezzi, and M. Tubino (2007), Monitoring and predicting channel change in a free-evolving, small Alpine river: Ridanna Creek (North East Italy), *Earth Surface Processes and Landforms*, *32*(14), 2104-2119, doi:10.1002/esp.1511.

Mao, L., L. Picco, M. A. Lenzi, and N. Surian (2017), Bed material transport estimate in large gravel-bed rivers using the virtual velocity approach, *Earth Surface Processes and Landforms*, *42*(4), 595-611, doi:10.1002/esp.4000.

Mao, L., and N. Surian (2010), Observations on sediment mobility in a large gravel-bed river, *Geomorphology*, *114*(3), 326-337, doi:10.1016/j.geomorph.2009.07.015.

Meunier, P., F. Métivier, E. Lajeunesse, A. S. Mériaux, and J. Faure (2006), Flow pattern and sediment transport in a braided river: The “torrent de St Pierre” (French Alps), *Journal of Hydrology*, *330*(3-4), 496-505, doi:10.1016/j.jhydrol.2006.04.009.

Middleton, L., P. Ashmore, P. Leduc, and D. Sjogren (2019), Rates of planimetric change in a proglacial gravel-bed braided river: Field measurement and physical modelling, *Earth Surface Processes and Landforms*, *44*(3), 752-765, doi:10.1002/esp.4528.

Milan, D. J., G. L. Heritage, and D. Hetherington (2007), Application of a 3D laser scanner in the assessment of erosion and deposition volumes and channel change in a proglacial river, *Earth Surface Processes and Landforms*, *32*(11), 1657-1674, doi:10.1002/esp.1592.

Montgomery, D. R., and J. M. Buffington (1997), Channel-reach morphology in mountain drainage basins, *Geological Society of America Bulletin*, *109*(5), 596-611.

Navratil, O., F. Liébault, H. Bellot, E. Travaglini, J. Theule, G. Chambon, and D. Laigle (2013), High-frequency monitoring of debris-flow propagation along the Réal Torrent, Southern French Prealps, *Geomorphology*, *201*, 157-171, doi:10.1016/j.geomorph.2013.06.017.

Nicholas, A. P. (2000), Modelling bedload yield in braided gravel bed rivers, *Geomorphology*, *36*(1-2), 89-106, doi:Doi 10.1016/S0169-555x(00)00050-7.

Paola, C. (1996), *Incoherent structures: Turbulence as a metaphor for stream braiding, in Coherent Flow Structures in Open Channels*, John Wiley, Chichester. ed.

Peirce, S., P. Ashmore, and P. Leduc (2018), The variability in the morphological active width: Results from physical models of gravel-bed braided rivers, *Earth Surface Processes and Landforms*, *43*(11), 2371-2383, doi:10.1002/esp.4400.

Piégay, H., F. Arnaud, M. Cassel, T. Dépret, A. Alber, K. Michel, A.-J. Rollet, and L. Vaudor (2016), Suivi par RFID de la mobilité des galets : Retour sur 10 ans d'expérience en grandes rivières, *Bulletin de la Societe Royale des Sciences de Liege 67*, 77-91.

Piton, G., and A. Recking (2017), The concept of travelling bedload and its consequences for bedload computation in mountain streams, *Earth Surface Processes and Landforms*, *42*(10), 1505-1519, doi:10.1002/esp.4105.

Pryor, B. S., T. Lisle, D. S. Montoya, and S. Hilton (2011), Transport and storage of bed material in a gravel-bed channel during episodes of aggradation and degradation: a field and flume study, *Earth Surface Processes and Landforms*, *36*(15), 2028-2041, doi:10.1002/esp.2224.

Recking, A. (2013a), An analysis of nonlinearity effects on bed load transport prediction, *Journal of Geophysical Research: Earth Surface*, *118*(3), 1264-1281, doi:10.1002/jgrf.20090.

Recking, A. (2013b), Simple Method for Calculating Reach-Averaged Bed-Load Transport, *Journal of Hydraulic Engineering*, *139*, doi:10.1061/ (ASCE)HY.1943-7900.0000653.

Recking, A., P. Frey, A. Paquier, and P. Belleudy (2009), An experimental investigation of mechanisms involved in bed load sheet production and migration, *Journal of Geophysical Research*, *114*(F3), doi:10.1029/2008jf000990.

Recking, A., G. Piton, D. Vazquez-Tarrio, and G. Parker (2016), Quantifying the Morphological Print of Bedload Transport, *Earth Surface Processes and Landforms*, *41*(6), 809-822, doi:10.1002/esp.3869.

Rickenmann, D., and A. Recking (2011), Evaluation of flow resistance in gravel-bed rivers through a large field data set, *Water Resources Research*, *47*(7), n/a-n/a, doi:10.1029/2010wr009793.

Roth, D. L., E. E. Brodsky, N. J. Finnegan, D. Rickenmann, J. M. Turowski, and A. Badoux (2016), Bed load sediment transport inferred from seismic signals near a river, *Journal of Geophysical Research: Earth Surface*, *121*(4), 725-747, doi:10.1002/2015jf003782.

Surian, N. (2015), Fluvial Processes in Braided Rivers, edited, pp. 403-425, doi:10.1007/978-3-319-17719-9_15.

Tsai, V. C., B. Minchew, M. P. Lamb, and J.-P. Ampuero (2012), A physical model for seismic noise generation from sediment transport in rivers, *Geophysical Research Letters*, *39*(2), n/a-n/a, doi:10.1029/2011gl050255.

Vázquez-Tarrío, D., A. Recking, F. Liébault, M. Tal, and R. Menéndez-Duarte (2018), Particle transport in gravel-bed rivers: Revisiting passive tracer data, *Earth Surf. Process. Landforms*, doi:10.1002/esp.4484.

Vericat, D., J. M. Wheaton, and J. Brasington (2017), Revisiting the Morphological Approach, in *Gravel-Bed Rivers*, edited, pp. 121-158, doi:10.1002/9781118971437.ch5.

Warburton, J. (1992), Observations of Bed Load Transport and Channel Bed Changes in a Proglacial Mountain Stream, *Arctic and Alpine Research*, *24*(3), doi:10.2307/1551657.

Warburton, J. (1994), Channel change in relation to meltwater flooding, Bas Glacier d'Arolla, Switzerland, *Geomorphology*, *11*, 141-149, doi:0169-555X/94/$07.00.

Warburton, J., and T. Davies (1994), Variability of bedload transport and channel morphology in a braided river hydraulic model, *Earth Surface Processes and Landforms*, *19*(5), 403-421, doi:10.1002/esp.3290190503.

Wilkinson, S. N., I. P. Prosser, and A. O. Hughes (2006), Predicting the distribution of bed material accumulation using river network sediment budgets, *Water Resources Research*, *42*(10), doi:Artn W10419 10.1029/2006wr004958.

Williams, R. D., J. Brasington, M. Hicks, R. Measures, C. D. Rennie, and D. Vericat (2013), Hydraulic validation of two-dimensional simulations of braided river flow with spatially continuous aDcp data, *Water Resources Research*, *49*(9), 5183-5205, doi:10.1002/wrcr.20391.

Williams, R. D., J. Brasington, D. Vericat, and D. M. Hicks (2014), Hyperscale terrain modelling of braided rivers: fusing mobile terrestrial laser scanning and optical bathymetric mapping, *Earth Surface Processes and Landforms*, *39*(2), 167-183, doi:10.1002/esp.3437.

Williams, R. D., R. Measures, D. M. Hicks, and J. Brasington (2016), Assessment of a numerical model to reproduce event-scale erosion and deposition distributions in a braided river, *Water Resour Res*, *52*(8), 6621-6642, doi:10.1002/2015WR018491.

Williams, R. D., C. D. Rennie, J. Brasington, D. M. Hicks, and D. Vericat (2015), Linking the spatial distribution of bed load transport to morphological change during high-flow events in a shallow braided river, *Journal of Geophysical Research: Earth Surface*, *120*(3), 604-622, doi:10.1002/2014jf003346.

APPENDIX A

HYDRAULICS CALCULATION

To estimate the main hydraulics parameters (velocity, hydraulic radius and water depth) at a given cross section from the measured discharge Q, we used the Ferguson (2007) flow resistance equation in an iterative way:

$$\frac{U}{\sqrt{gR_hS}} = \frac{2.5\frac{R_h}{D_{84}}}{\sqrt{1 + 0.15\left(\frac{R_h}{D_{84}}\right)^{5/3}}} \qquad \text{(A.1)}$$

Where S (-) is the river bed slope, D_{84} (m) the 84% percentile of the grain size distribution, R_h (m) the hydraulic radius, U (m s^{-1}) the mean flow velocity and g (m s^{-2}) the gravity acceleration.

It was then possible to estimate a local or an average Shield number ($\tau_{84}{}^*$) with respectively the local water depth (d) in the cross section or an averaged hydraulic radius (R_h) in the main channel:

$$\tau_{84}{}^* = \frac{\rho g d S}{(\rho_s - \rho) g D_{84}} \quad \text{(A.2)}$$

Where ρ is the water density, ρ_s is the sediment density. This method was used to compare the bed mobility associated to morphological changes between the beginning and the end of the campaign.

APPENDIX B

BED LOAD CALCULATION

Many equations have been proposed in the literature and could be used to predict bedload. To test where bedload calculation should be used in alternatively braiding and confined sections, we choose to test the one proposed in Recking (2010), Recking (2013) and Recking *et al.* (2016), Eq.(B.1) and Eq.(B.2). It was specifically developed from field data for reach average computation and was validated with a large independent data set. The input parameters are Q, W, S, D_{50} and D_{84}.

$$q_b{}^* = \frac{q_b}{\rho_s \sqrt{g(s-1){D_{84}}^3}} = \frac{14{\tau^*}^{2.5}}{1 + \left(\frac{\tau_m^*}{\tau^*}\right)^4} \quad \text{(B.1)}$$

where q_b (kg s^{-1} m^{-1}) is the unit bedload transport per unit width, $s = \rho_s/\rho$, ρ_s is the sediment density, ρ is the water density, and g is the gravity acceleration. In Eq. B.1 the parameter τ_m^* defines the transition between partial transport and full mobility. It depends

on the morphology of the stream [*Recking et al.*, 2016] and was calculated using the following equation:

$$\tau_m^* = 1.5S^{0.75} \quad \text{(B.2)}$$

This formula was used with the averaged hydraulics parameters in the main active channel (calculations were made on the website: www.bedloadweb.com). The percentages of well predicted values that fell in a given range were calculated considering a range [0.1-10] (E10), [0.2-5] (E5) and [0.5-2] (E2) as often done to evaluate sediment transport formula.

APPENDIX C

RESAMPLING TECHNIQUE TO DETECT TEMPORAL TREND ON BEDLOAD SAMPLING

To test the significance of a temporal trend in bedload transport flux, the following resampling procedure was adopted on the bedload samples (N=60):

i) 5000 selections of N_r random samples are performed (N_r<N),

ii) For each random selection, a log-linear model is fitted between the N_r bedload rates and flow rates,

iii) For each regression, a linear model is fitted between the residuals and the time,

iv) The significance of this relation of residuals through time is analyzed through its p_{value}. The temporal trend is considered significant if the 5000 p_{values} obtained are lower than 0.05,

v) These steps are repeated by varying N_r from 59 to 40.